FLAgellum Member 8 modulates extravasation and extravascular distribution of African trypanosomes.

Estefanía Calvo Alvarez[1]*, Jean Marc Tsagmo Ngoune[1], Anneli Cooper[2], Christelle Travaillé[1,3], Aline Crouzols[1], Annette MacLeod[2] and Brice Rotureau*[1,4]

[1] Trypanosome Transmission Group, Trypanosome Cell Biology Unit, INSERM U1201, Department of Parasites and Insect Vectors, Institut Pasteur, Université Paris Cité, Paris, France.

[2] Wellcome Centre for Integrative Parasitology, College of Medical, Veterinary, and Life Sciences, Henry Wellcome Building for Comparative Medical Sciences, Glasgow, Scotland, United Kingdom.

[3] Photonic BioImaging (UTechS PBI), Institut Pasteur, Université Paris Cité, Paris, France.

[4] Parasitology Unit, Institut Pasteur of Guinea, Conakry, Guinea.

*Corresponding authors:

estefaniacalvoalvarez@gmail.com & brice.rotureau@pasteur.fr

Keywords: *Trypanosoma brucei*, FLAM8, flagellum, extravasation, dissemination, sensing

Short title: FLAM8 modulates extravascular trypanosome dissemination

6 Figures, 3 Supplementary Figures and 1 Supplementary Table

Abstract (231/300 words)

In the mammalian host, the biology of tissue-dwelling *Trypanosoma brucei* parasites is not completely understood, especially the mechanisms involved in their extravascular colonization. The trypanosome flagellum is an essential organelle in multiple aspects of the parasites' development. The flagellar protein termed FLAgellar Member 8 (FLAM8) acts as a docking platform for a pool of Cyclic AMP response protein 3 (CARP3) that is involved in signaling. FLAM8 exhibits a stage-specific distribution suggesting specific functions in the mammalian and vector stages of the parasite. Analyses of knockdown and knockout trypanosomes in their mammalian forms demonstrated that FLAM8 is not essential *in vitro* for survival, growth, motility and stumpy differentiation. Functional investigations in experimental infections showed that *FLAM8*-deprived trypanosomes can establish and maintain an infection in the blood circulation and differentiate into insect transmissible forms. However, quantitative bioluminescence imaging and gene expression analysis revealed that *FLAM8*-null parasites exhibit a significantly impaired dissemination in the extravascular compartment, that is restored by the addition of a single rescue copy of *FLAM8*. *In vitro* trans-endothelial migration assays revealed significant defects in trypanosomes lacking *FLAM8*, possibly due to cAMP signaling impairments when a pool of CARP3 is not stabilized within FLAM8-related scaffold. FLAM8 is the first flagellar component shown to modulate *T. brucei* distribution in the host tissues, possibly through sensing functions, contributing to the maintenance of extravascular parasite populations in mammalian anatomical niches, especially in the skin.

Author Summary (192/200 words)

Trypanosoma brucei parasites cause neglected tropical diseases termed human and animal African trypanosomiases. Transmitted by the bite of an infected tsetse fly, upon deposition in the skin of a mammalian host, these parasites occupy both the vasculature and extravascular tissues. Currently, the biology of tissue-resident parasites is not well understood, and the parasite factors that mediate extravascular colonization are not known. Using quantitative *in vivo* bioluminescence imaging and *ex vivo* gene expression quantification in host infected tissues and blood, we reveal that the flagellar parasite protein FLAM8 modulates the extravascular dissemination of trypanosomes in the mammalian host. FLAM8 is known to act as a docking platform for signaling complexes in the flagellum, but we observe that it does not influence parasite differentiation into transmissible stages. However, we show that the absence of FLAM8 results in the loss of a key component of the flagellar adenylate cyclase signaling complexes, and reduces parasite migration through endothelial cell monolayers, suggesting that FLAM8 is important for parasite exchanges between the intravascular and the extravascular compartments. This work identifies a key trypanosome flagellar component involved in host-parasite interactions, including the modulation of parasite tropism and extravascular dissemination.

66 **Introduction**

67 *Trypanosoma brucei* is an extracellular parasite responsible for African
68 trypanosomiases, including sleeping sickness in humans and *nagana* in cattle. African
69 trypanosomes are blood and tissue-dwelling protists transmitted by the bite of the
70 blood-feeding tsetse fly (*Glossina* genus). In the mammalian host, parasites face
71 different micro-environments, including deadly challenges by multiple types of host
72 immune responses and variable availability of carbon sources. This requires major
73 morphological and metabolic adaptations, driven by the activation of specific gene
74 expression programs, that are critical for life-cycle progression [1-3]. Recently, the
75 importance of extravascular tropism for *T. brucei* has been re-discovered in animal
76 models: in addition to the brain, parasites occupy most mammalian tissues, especially
77 the skin and the adipose tissues [4-7]. However, the role of extravasation and
78 sequestration of trypanosomes in specific anatomical niches and the underlying
79 molecular processes are not understood yet.

80 The trypanosome flagellum is an essential organelle anchored along the surface of the
81 cell body and present in all stages of its development [8]. It is essential for parasite
82 viability [9], cell division and morphogenesis [10], attachment to the tsetse salivary
83 glands [11] and motility [12]. In the insect host, the flagellum remains at the forefront
84 of the cell and is likely to be involved in sensory and signaling functions required for
85 host-parasite interactions [13, 14]. In the mammalian host, flagellar motility was shown
86 to be critical for establishment and maintenance of bloodstream infection [15].
87 Nevertheless, the contributions of the trypanosome flagellum to parasite tropism and
88 spatiotemporal dissemination outside vessels in the mammalian host remained to be
89 explored.

90 A proteomic analysis of intact flagella purified from the insect stage of the parasite
91 identified a group of flagellar membrane and matrix proteins with unique patterns and
92 dynamics [16]. Amongst them, one large protein (3,075 amino acids) termed FLAgellar
93 Member 8 (FLAM8) is present only at the distal tip of the flagellum in the insect
94 procyclic form [16-18]. Interestingly, FLAM8 is redistributed along the entire length of
95 the flagellum in mammalian forms, including in stumpy transmissible stages [19], which
96 may imply a stage-specific function for this protein. Therefore, we hypothesized that
97 FLAM8 could be involved in host-parasite interactions or in developmental
98 morphogenesis. Here, we investigated the roles of FLAM8 in mammalian form
99 parasites *in vitro* in terms of survival, proliferation, motility, and differentiation, as well
100 as the *in vivo* dynamics of the intravascular and extravascular parasite burden over
101 the course of murine infection. Intriguingly, experimental infections in mice monitored
102 and quantified by bioluminescence imaging and gene expression analyses
103 demonstrated the involvement of FLAM8 in parasite dissemination in the extravascular
104 compartments. In addition, *in vitro* transmigration studies detected impaired
105 extravasation ability of *FLAM8*-deprived parasites, possibly resulting from the loss of
106 components of flagellar adenylate cyclase signaling complexes.

107 **Results**

108 ***FLAM8* RNAi silencing does not affect parasite survival**

109 The differential distribution of FLAM8 in the flagellum of the different trypanosome
110 stages [19] raises the question of its specific functions during the parasite cycle. To
111 investigate the potential role(s) of FLAM8 in the mammalian host, bloodstream form
112 parasites were first engineered for inducible RNAi knockdown of *FLAM8* in a
113 monomorphic strain expressing a mNeonGreen-tagged version of FLAM8. In order to
114 monitor their behavior in mouse by whole-body imaging approaches, these
115 *FLAM8::mNG FLAM8*^{RNAi} mutants were subsequently transformed to overexpress a
116 chimeric triple reporter protein [20]. Upon RNAi induction with tetracycline for 72 h *in*
117 *vitro*, *FLAM8* expression was reduced by 60% at the mRNA level (Fig. 1A) and became
118 undetectable at the protein level by immunofluorescence (Fig. 1B). Parasite growth
119 was monitored over 6 days upon induction of RNAi and no impact on proliferation was
120 observed (Fig. 1C), which suggests that FLAM8 is possibly not essential for survival of
121 mammalian forms of the parasite in cell culture conditions.

122 Then, the linear correlation between the emitted bioluminescence and the number of
123 parasites was assessed in an IVIS Spectrum imager prior to *in vivo* challenge (Fig.
124 S1). To get insights into the function of FLAM8 in the mammalian host, groups of male
125 BALB/c mice were infected by the intraperitoneal route with 10^5 parasites of the
126 parental, non-induced and induced cell lines (Fig. 1D). *In vivo* RNAi silencing of *FLAM8*
127 was maintained in mice by the addition of doxycycline in sugared drinking water 48 h
128 prior infection and until the end of the experiment. The course of the infection was
129 monitored daily by i) quantifying the parasitemia, and ii) acquiring the bioluminescent
130 signal emitted by the parasites in the entire organism with an IVIS Spectrum imager.
131 The number of parasites in the extravascular compartment at a given timepoint can be

132 extrapolated by subtracting the known number of trypanosomes in the vascular system
133 (parasitemia x blood volume, according to body weight) from the total number of
134 parasites in the organism (total bioluminescence). No differences were detected,
135 neither in the establishment of the infection and the subsequent variations in the
136 number of intravascular parasites (Fig. 1E, IV), nor in the number of parasites
137 occupying extravascular tissues (Fig. 1F, EV). Similar population profiles were
138 observed over the course of the infection for both intra- and extravascular parasites in
139 each of the three independent groups of infected mice (Fig. 1D-F). In the extravascular
140 compartment, no significant differences were detected in terms of parasite
141 dissemination over the entire animal body in any group (Fig. 1G).

142 ***FLAM8* knockout does not affect trypanosome growth *in vitro***

143 Considering that i) *FLAM8* RNAi silencing efficiency was only partial (40% *FLAM8*
144 mRNA left after 72 h of induction), ii) the efficacy of doxycycline-induced *FLAM8*
145 repression could have been even lower *in vivo*, and that iii) the parental strain used for
146 this first strategy was monomorphic (i.e. unable to differentiate into tsetse adapted
147 stumpy stages), we reasoned that a gene knockout approach in a pleomorphic strain
148 would be more appropriate to evaluate the potential role(s) of FLAM8 during the
149 mammalian host infection. Therefore, a Δ*FLAM8* knockout cell line was generated in
150 pleomorphic trypanosomes by homologous recombination. The full replacement of one
151 *FLAM8* allele and the partial replacement of the second one (to allow the use of a
152 shorter *in situ* rescue sequence than the long *FLAM8* coding sequence) by distinct
153 resistance cassettes was verified by whole-genome sequencing and PCR (Fig. S2).
154 The absence of full or truncated FLAM8 protein expression was further assessed by
155 immunofluorescence analysis with an anti-FLAM8 antibody [19] targeting the region of
156 FLAM8 that was not replaced in the second allele (Fig. 2A). This was also confirmed

157 at the mRNA level by RT-qPCR (Table S1). The trypanosome cell lines generated
158 were further transformed to express the chimeric triple reporter construct [20], and the
159 linear correlation between the bioluminescence signal and the total number of
160 parasites was analyzed for all strains both *in vitro* and *in vivo* (Fig. S3). In Δ*FLAM8*
161 knockout parasites where a rescue copy of one *FLAM8* allele was added back into its
162 endogenous locus, the FLAM8 distribution was restored along most of the flagellum
163 length, as assessed by immunofluorescence analysis (Fig. 2A). No impact on parasite
164 growth in culture conditions was observed (Fig. 2B). Next, we investigated whether the
165 loss of FLAM8 could have impacted the total length of the flagellum based on the
166 measurement of the signal obtained with the axonemal marker mAb25: no difference
167 was observed among BSF lines (Fig. 2C). In addition, the absence of *FLAM8* did not
168 affect parasite speed or linearity *in vitro*, neither in terms of speed nor in linearity (Fig.
169 2D-E). Compatible with our previous observations after RNAi silencing, these results
170 show that pleomorphic trypanosomes tolerated the loss of *FLAM8 in vitro*.

171 ***FLAM8* knockout affects trypanosome distribution in the mammalian host**

172 Then, functional investigations in the mammalian host were performed by infecting
173 BALB/c mice either with the pleomorphic parental strain, three distinct Δ*FLAM8*
174 knockout subclones (resulting from independent recombination events) or one
175 Δ*FLAM8* strain bearing a rescue copy of *FLAM8* (Fig. 3). The infections were
176 monitored daily for 4 weeks by quantifying the parasitemia and the bioluminescence
177 signals emitted from whole animals (Fig. 3A). Null mutant parasites were able to
178 establish an infection in the bloodstream as well as in the extravascular compartment.
179 Within the vasculature, the overall amounts of parasites throughout the whole
180 experimental infection were comparable in all strains (Fig. 3B), yet with a slightly lower
181 parasitemia observed at the first peak of parasitemia in mice infected with the three

182 Δ*FLAM8* subclones as compared to mice infected with the parental strain (Fig. 3B). On
183 the other hand, quantitative analyses of extravascular parasites showed a different
184 scenario. Unlike in the intravascular compartment, significantly lower numbers of
185 extravascular trypanosomes were observed between day 5 to 12, and from day 19
186 post-infection until the end of the experiment at day 27, evidencing an impaired
187 extravascular colonization for Δ*FLAM8* parasites as compared to parental controls
188 (Fig. 3C). To note, distribution profiles of all pleomorphic strains were different from
189 those observed in mice infected with monomorphic parasites: larger amounts of
190 trypanosomes were seen occupying the extravascular compartment reaching up to 5-
191 $8x10^9$ parasites, while the maximum amount found in the bloodstream never exceeded
192 $7x10^7$ trypanosomes (Fig. 3B and C, respectively).
193 Furthermore, quantification of the parasite spreading over the whole animal bodies
194 showed that the depletion of *FLAM8* resulted in significantly impaired dissemination of
195 Δ*FLAM8* null mutant parasites in the extravascular compartment (days 5 to 13, 19 and
196 27 post-infection). This was mostly restored in trypanosomes bearing a rescue copy of
197 *FLAM8* (Fig. 3D).

198 ***FLAM8* knockout impairs extravascular trypanosome dissemination**

199 We reasoned that the accuracy of the intra- Vs. extravascular parasite population
200 estimation from bioluminescence detection on small regions of interest could be
201 limited. Therefore, the same experiment was repeated, with comparable trends in
202 terms of extravascular parasite populations and parasite dissemination according to
203 the strain (Fig. 4A-C). At the end of this second experimental challenge (Day 24),
204 trypanosomes were removed from the vascular system by saline perfusion prior to
205 organ dissection. Individual organs were then collected for quantifying the expression
206 of different parasite genes by RT-qPCR. First, the absence of *FLAM8* transcripts was

207 confirmed in animals infected with Δ*FLAM8* parasites, whereas FLAM8 mRNAs were
208 detected in mice infected with both the parental and rescue strains (Table S1).
209 Normalized *Tubulin* expression was then used to compare the parasite densities
210 between organs and strains (Fig. 4D-E). In all mice, the highest number of
211 extravascular parasites was observed in the skin. In all organs, a marked decrease in
212 the number extravascular parasites was detected from mice infected with Δ*FLAM8*
213 parasites as compared to mice infected by parental and rescue parasites (Fig. 4D).
214 When considering the average difference between the number of parasites in organs
215 versus blood by strains, the statistically significant decrease in extravascular FLAM8-
216 deprived parasite densities appeared even more clearly (Fig. 4E). The rescue cell line
217 recapitulated EV parasite profiles in all organs examined with an average delta that
218 was not statistically different from the parental line.
219 We reasoned that this reduced extravascular dissemination of FLAM8-deprived
220 parasites could possibly be due to: (1) a lower proliferation rate, (2) a defect in motility,
221 (3) a higher rate of differentiation into non-proliferative stumpy forms, and / or (4) an
222 extravasation defect. The two first hypotheses could immediately be discarded as no
223 difference was observed between strains, neither in cell growth *in vitro* (Fig. 2B) and
224 *in vivo* (Fig. 3B and 4A), nor in cell motility *in vitro* (Fig. 2D-E). The two last hypotheses
225 were then successively tested.

226 **The absence of FLAM8 does not affect parasite differentiation**

227 The systemic reduction in the extravascular Δ*FLAM8* parasite population could result
228 from a disequilibrium in the parasite differentiation into non-proliferative transmissible
229 forms. Therefore, we assessed whether the absence of FLAM8 could have impacted
230 the differentiation of proliferative slender into transmissible stumpy forms in the blood
231 and organs by immunofluorescence or RT-qPCR. In cultured parasites, the absence

232 of *FLAM8* did not significantly alter differentiation (Fig. 5A-B), and freshly differentiated
233 *FLAM8*-deprived stumpy parasites were able to further differentiate and maintain *in*
234 *vitro* as procyclic trypanosomes, as were the parental and rescue strains (Fig. 5C-D).
235 *In vivo*, the natural differentiation of proliferative slender into non-proliferative stumpy
236 parasites was confirmed by anti-PAD1 immunofluorescence staining of blood sampled
237 at the first peak of parasitemia (Fig. 5E, Day 5 of the first *in vivo* challenge), as well as
238 by RT-qPCR on blood and dissected organs at the end of the experiment (Fig. 5F, Day
239 24 of the second *in vivo* challenge). For each sample, *Tubulin* expression was used to
240 normalize the *PAD1* mRNA levels to compare the average levels of parasites
241 expressing *PAD1* mRNAs over the total parasite populations between organs and
242 strains (Fig. 5F), with a higher Delta CqPAD1-CqTub correlating with a lower amount
243 of *PAD1* transcripts in the organ. *PAD1* transcripts were detected in each organ at
244 least in one individual, showing that all tested organs represent a suitable environment
245 for the parasites to differentiate into transmissible forms (Fig. 5F). In mice infected with
246 the parental and rescue strains, the highest levels of *PAD1* transcripts were detected
247 in blood and skin, suggesting an accumulation or an increased rate of differentiation in
248 organs directly involved in parasite transmission. No *PAD1* transcripts were detected
249 in the gut, liver and spleen in mice infected with the parental and rescue strains,
250 whereas *PAD1* transcripts were detected in these three organs from mice infected with
251 the Δ*FLAM8* strains. However, when considering the average Delta CqPAD1-CqTub
252 in the entire organisms by strains, the relative proportions of parasites expressing
253 *PAD1* mRNAs were not significantly different among groups, confirming that FLAM8 is
254 not involved in parasite differentiation (Fig. 5F).

255 **Parasite extravasation is impaired in *FLAM8*-deprived trypanosomes**

256 To test the last hypothesis, we asked whether the absence of FLAM8 might influence
257 the way parasites traverse the vessel walls to access extravascular tissues. We first
258 established a transmigration assay using human umbilical vein endothelial cells
259 (HUVECs) grown to confluence on polyester transwell inserts with 3 µM pores,
260 separating two chambers to mimic the vascular endothelium *in vitro* (Fig. 6A). Once
261 HUVECs have reached confluence, 10^6 parental, *FLAM8*-deprived or rescue
262 trypanosomes were added to the upper chamber and incubated for 24h. The number
263 of trypanosomes that migrated through the endothelial monolayer into the lower
264 chamber and the number of non-migrating trypanosomes remaining in the upper
265 chamber of the transwell system were counted by flow cytometry to determine the
266 transmigration percentage. Interestingly, all *FLAM8*-knockout subclones showed a
267 significant reduction in transmigration relative to parental controls (25,6%, 70,7% and
268 33,8% of parasites crossing for KO1, 2 and 3, respectively) (Fig. 6B). Rescue
269 trypanosomes expressing only one *FLAM8* allele exhibited an intermediate
270 transmigration phenotype in which 59,2% of the parasites migrated through the
271 endothelial monolayer (Fig. 6B), which was lower than for parental trypanosomes but
272 significantly higher than for KO1 and KO3 null mutants (Fig. 6B). This demonstrates a
273 strong impairment of parasites lacking *FLAM8* to cross through a confluent layer of
274 endothelial cells, which was partially restored in rescue parasites.

275 Knowing that, in mammalian forms, FLAM8 was recently identified to be part of a
276 flagellar complex including the cyclic AMP response protein 3 (CARP3) [21], we
277 reasoned that this trans-endothelial crossing impairment could be caused by a defect
278 in sensing and / or signaling. To assess how the absence of FLAM8 was impacting
279 CARP3 localization and/or abundance, CARP3 was imaged by IFA in all strains (Fig.

280 6C). As expected, CARP3 was detected in a punctiform pattern along the entire
281 flagellum length in parental mammalian forms, but not in Δ*FLAM8* parasites, and the
282 presence of a *FLAM8* rescue copy in Δ*FLAM8* parasites restored the detection of
283 CARP3, yet in lower amounts than in parental cells (Fig. 6C).
284
285 In total, these data show that FLAM8 is likely involved in a cellular pathway modulating
286 trypanosome extravasation and consequently trypanosome dissemination in the
287 extravascular compartment of the mammalian host.

288 **Discussion**

289 The differential localization of FLAM8 from the very distal tip in tsetse midgut procyclic
290 parasites to the entire flagellum length in the mammalian-infectious stages [19]
291 prompted us to speculate that FLAM8 could play a distinct and specific role in each
292 host. Here, we present for the first time the connection of a flagellar protein with the
293 efficiency of trypanosomes to disseminate outside the mammalian host vasculature,
294 especially in the skin. Quantitative analyses of experimental animal infections
295 monitored by bioluminescence imaging and gene expression analysis showed that the
296 absence of FLAM8 impairs parasite extravasation and dissemination in the host
297 extravascular compartment over the time of the infection, which was mostly recovered
298 by the integration of a single rescue copy of the *FLAM8* gene in the endogenous locus.

299 **1. FLAM8 and trypanosome transmission**

300 In the bloodstream, the balance between proliferative slender parasites and tsetse-
301 adapted stumpy forms responds to a quorum sensing mechanism involving the
302 production of oligopeptides and their reception through a specific transporter [22]. The
303 absence of FLAM8 did not alter the ability of the parasites to differentiate into
304 transmissible stumpy forms at the two observed time points (first peak of parasitemia
305 and 3 weeks after infection). Although stumpy proportions were not evaluated over the
306 entire course of the infection, this evidence suggests that FLAM8 does not play an
307 integral role in this process. In addition, the retained ability of *FLAM8*-deprived stumpy
308 cells to differentiate into procyclic forms *in vitro* suggests that they could further pursue
309 their cyclical development upon ingestion by a tsetse fly.

310 Extravascular trypanosomes occupy the interstitial space of several organs, including
311 the central nervous system, testes, adipose tissues, and skin [4-7, 23-25]. The
312 relevance of skin-dwelling trypanosomes in parasite transmission has been

313 demonstrated by xenodiagnosis experiments, early after the infective bite [26], or later
314 in the infection [4], even in the absence of detectable parasitemia. More recently, the
315 presence of extravascular trypanosomes was confirmed in the skin of confirmed and
316 suspected cases of sleeping sickness [27]. Here, we show that all tested organs
317 represent a suitable environment for the parasites to differentiate into transmissible
318 forms, yet the highest amounts of *PAD1* transcripts were detected in blood and skin,
319 suggesting an increased rate of differentiation, or an accumulation of differentiated
320 stumpy forms in organs directly involved in parasite transmission. In total, the impaired
321 spreading of *FLAM8*-null parasites over the extravascular compartment would
322 mathematically reduce the probability for parasites to be ingested by tsetse flies. This
323 could be especially significant for the skin, that has the highest parasite density, and
324 the highest overall parasite load due to its size, at the direct interface with insect
325 vectors.

326 **2. On the possible cellular function(s) of FLAM8**

327 Proliferative slender trypanosomes are highly mobile [28] and this motility was proved
328 to influence virulence *in vivo*. For instance, the lack of propulsive motility in flagellar
329 dynein light chain 1 (*LC1*) knockout mutants resulted in the inability of trypanosomes
330 to establish an infection in the bloodstream [15]. Here, *FLAM8* depletion in pleomorphic
331 mammalian forms did not alter parasite growth and cell motility in matrix-containing
332 medium. However, quantitative analyses showed that *FLAM8*-null trypanosomes were
333 less numerous in extravascular tissues as compared to parental controls. Assuming
334 that parasite motility could be different in tissues and interstitial spaces with biophysical
335 properties distinct from those in the blood [28, 29], one cannot exclude that the motility
336 of Δ*FLAM8* knockout parasites might be somehow altered in the extravascular

337 compartment. Intravital imaging for motility analyses at the cell level would be needed
338 to confirm this hypothesis.
339 Historically, most studies on *T. brucei* virulence in experimental infections have
340 considered the blood circulation almost as the sole host compartment parasitized by
341 trypanosomes, whereas extravascular parasite niches and the underlying exchanges
342 between both compartments have been underestimated for long. De Niz and
343 colleagues recently identified adhesion molecules as key players for tissue tropism
344 [30]. They showed that reservoir establishment happens before vascular permeability
345 is compromised, suggesting that extravasation is an active mechanism, and depends
346 on trypanosome interactions with endothelial surface adhesion molecules, such as E-
347 selectin, P-selectins, or ICAM2 [30]. Here, we showed that the absence of FLAM8 led
348 to a strong impairment in parasite extravasation. The fact that *FLAM8*-null
349 trypanosomes were not able to disseminate properly over the extravascular
350 compartment could somehow imply defects in the way parasites sense their
351 microenvironment or interact with the host endothelial cells, resulting in an alteration
352 of their extravascular tropism.
353 The insect forms´ coordinated social motility *in vitro* is linked to cAMP signaling at the
354 flagellar tip [31, 32], i. e. where FLAM8 localizes [19]. The architecture of an adenylate
355 cyclase complex in the tip nanodomain was recently shown to be essential for social
356 motility and salivary gland colonization [21]. In this complex, CARP3 interacts with the
357 catalytic domain of adenylate cyclases and regulates abundance of multiple adenylate
358 cyclase isoforms. We recently demonstrated that the CARP3 tip localization depends
359 on the presence of FLAM8 acting as a scaffold protein [21]. Thus, trypanosome
360 migration and transmission in the tsetse vector specifically depend on adenylate
361 cyclase complex-mediated signaling in the tip nanodomain including FLAM8 [21].

362 Interestingly, we have recently shown that CARP3 and FLAM8 are both redistributed
363 along the entire length of the flagellum during their differentiation to the mammalian
364 stage, and that they further remain associated in flagellar complexes in mammalian
365 forms [21]. Here, this was confirmed by the absence of CARP3 from the flagellum of
366 FLAM8-deprived mammalian forms. Altogether, these data may imply a stage-specific
367 function of CARP3-containing signaling complexes depending on FLAM8 for their sub-
368 flagellar localization. Environmental sensing and / or signaling, possibly through direct
369 contact with host cell receptors may play a role in extravasation. We propose that the
370 absence of FLAM8 would destabilize or delocalize these signaling complexes,
371 impairing parasite sensing, signaling and / or adhesion functions, hence preventing the
372 parasite to efficiently cross vascular endothelia.
373
374 To our knowledge, FLAM8 is the first flagellar component affecting parasite
375 extravasation and their subsequent dissemination in the extravascular host tissues *in*
376 *vivo*. Further investigations on the FLAM8 interactions with other possible partners in
377 the flagellum would help to unravel the roles of this fascinating and essential organelle,
378 especially regarding the modulation of trypanosome tropism, extravasation and
379 spreading in their mammalian hosts, and its implications in parasite virulence and
380 transmission.

381 **Materials and Methods**

382 **Strains, culture and *in vitro* differentiation**

383 The AnTat 1.1E Paris pleomorphic clone of *Trypanosoma brucei brucei* was derived
384 from a strain originally isolated from a bushbuck in Uganda in 1966 [33]. The
385 monomorphic *T. brucei* strain Lister 427 [34] was also used. All bloodstream forms
386 (BSF) were cultivated in HMI-11 medium supplemented with 10% (v/v) fetal bovine
387 serum (FBS) [35] at 37°C in 5% CO_2. For *in vitro* slender to stumpy BSF differentiation,
388 we used 8-pCPT-2′-O-Me-5′-AMP, a nucleotide analog of 5'-AMP from BIOLOG Life
389 Science Institute (Germany). Briefly, $2x10^6$ cultured pleomorphic AnTat 1.1E slender
390 forms were incubated with 8-pCPT-2′-O-Me-5′-AMP (5 µM) for 48 h [36]. For specific
391 experiments, *in vitro* differentiation of BSF into procyclic forms was performed by
392 transferring freshly differentiated short stumpy forms into SDM-79 medium
393 supplemented with 10% (v/v) FBS, 6 mM cis-aconitate and 20 mM glycerol at 27°C
394 [37].

395 Monomorphic BSF "Single Marker" (SM) trypanosomes are derivatives of the Lister
396 427 strain, antigenic type MITat 1.2, clone 221a [38], and express the T7 RNA
397 polymerase and tetracycline repressor. *FLAM8*^{RNAi} cells express complementary
398 single-stranded RNA corresponding to a fragment of the *FLAM8* gene from two
399 tetracycline-inducible T7 promoters facing each other in the pZJM vector [39]
400 integrated in the rDNA locus [40]. Addition of tetracycline (1 µg/mL) to the medium
401 induces expression of sense and anti-sense RNA strands that can anneal to form
402 double-stranded RNA (dsRNA) and trigger RNAi. For *in vivo* RNAi studies in mice,
403 doxycycline hyclate (Sigma Aldrich) was added in sugared drinking water (0.2 g/L
404 doxycycline hyclate combined with 50 g/L sucrose).

405 **Generation of FLAM8 RNAi mutants**

406 For the generation of the *FLAM8*^{RNAi} cell lines, a 380 bp (nucleotides 6665-7044)
407 fragment of *FLAM8* (Tb927.2.5760), flanked by 5' HindIII and 3' XhoI restriction sites
408 to facilitate subsequent cloning, was selected using the RNAit algorithm
409 (http://trypanofan.bioc.cam.ac.uk/software/RNAit.html) to ensure that the targeted
410 sequence was distinct from any other genes to avoid any cross-RNAi effects [41]. This
411 *FLAM8* DNA fragment was synthesized by GeneCust Europe (Dudelange,
412 Luxembourg) and inserted into the HindIII-XhoI digested pZJM vector [39].

413 The pZJM-FLAM8 plasmid was linearized with NotI prior to transfection using
414 nucleofector technology (Lonza, Italy) as described previously [42]. The cell line was
415 further engineered for endogenous tagging of *FLAM8* with an mNeonGreen (mNG) at
416 its C-terminal end by using the p3329 plasmid [43], carrying a *FLAM8* gene fragment
417 corresponding to *FLAM8* ORF nucleotides 8892-9391. Prior to nucleofection, NruI
418 linearization of p3329-FLAM8-mNG plasmid was performed.

419 For *in vivo* experiments in mice, *FLAM8*^{RNAi} parasites were finally modified by
420 integrating a plasmid encoding for the chimeric triple reporter which combines the red-
421 shifted firefly luciferase PpyREH9 and the tdTomato red fluorescent protein fused with
422 a TY1 tag [20]. Transformants were selected with the appropriate antibiotic
423 concentrations: phleomycin (1 µg/mL), blasticidin (5 µg/mL), G418 (2 µg/mL), and
424 puromycin (0.1 µg/mL). Clonal populations were obtained by limiting dilution. Cell
425 culture growth was monitored with an automatic Muse cell analyzer (Merck Millipore,
426 Paris).

427 **Generation of *FLAM8* KO mutants**

428 For generating the *FLAM8* knockout and rescue cell lines, all insert templates were
429 synthesized by GeneCust Europe (Dudelange, Luxembourg). For breaking the first

430 allele, the 300 first nucleotides of the *FLAM8* gene flanking sequences were added on
431 each side of a HYG resistance cassette (Fig. S2). For a complete disruption of the
432 *FLAM8* locus, a second selectable marker (PAC) was flanked with the *FLAM8*-flanking
433 sequence at 5' and by 300 nucleotides of the *FLAM8* ORF (nucleotides 501-800) at 3'.
434 For generating an add-back rescue cell line, due to the large size of the *FLAM8* ORF
435 (9,228 nucleotides), the PAC selection marker was replaced by a BLE marker cassette
436 flanked by the 300 first nucleotides of the *FLAM8* 5' untranslated region (UTR) and by
437 the nucleotides 1 to 500 of the *FLAM8* ORF for reinsertion into the endogenous locus
438 of the knockout cell line. PCR amplifications of the DNA fragments bearing the *FLAM8*
439 flanking sequences and the appropriate resistance markers were used for
440 nucleofection and generation of all cell lines. The primers used are listed below: 5'-
441 CATGACTTTACGTGTTTGGGCAC-3' (FW, located 82 bp upstream the flanking
442 5'UTR sequence); 5'-CTTGCTTGTTTCTGTTTCGCAAC-3' (RV, 130 bp downstream
443 the flanking 3'UTR sequence, used to replace one WT allele by HYG resistance
444 cassette); 5'- GCACACTAAAACTCATTGAAAGCC-3' (RV, 926 bp downstream the
445 ATG codon of *FLAM8*, used for second WT allele replacement by PAC cassette and
446 rescue line generation). All knockout and rescue cell lines were further transfected to
447 express the chimeric triple reporter protein PpyRE9H/TY1/tdTomato for multimodal *in*
448 *vivo* imaging approaches as described elsewhere [20]. Selection-marker recovery was
449 confirmed by screening individual clones in multi-well plates. Transformants were
450 selected with the appropriate antibiotic concentrations: phleomycin (1 µg/mL),
451 blasticidin (5 µg/mL), puromycin (0.1 µg/mL) and hygromycin (2.5 µg/mL). Clonal
452 populations were obtained by limiting dilution and cell culture growth was monitored
453 with an automatic Muse cell analyzer (Merck Millipore, Paris).

454 Knockout and rescue cell lines were validated by whole-genome sequencing (BGI,
455 Hong Kong). Briefly, genomic DNA from parental and mutant cell lines were sequenced
456 by the HiSeq4000 sequence system (Illumina), generating about 10 million 100-bp
457 reads and compared to that of the *T. brucei brucei* AnTat 1.1E Paris reference strain.
458 In addition, some validation of the construct integrations in mutants were performed by
459 PCR analysis according to standard protocols (Fig. S2 and Table 1).

460 **Table 1.** Oligonucleotides used for PCR validation of the Δ*FLAM8* knockout and rescue
461 cell lines.

Primer	Sequence	Target	
1	CATGACTTTACGTGTTTGGGCAC	*FLAM8* WT allele (82 nt upstream 5'UTR)	F
2	GCACACTAAAACTCATTGAAAGCC	*FLAM8* WT allele (926 nt downstream ATG)	R
3	CGTCCGAGGGCAAAGGAATAG	Hygromycin cassette	R
4	GACCGCGCACCTGGTGCATG	Puromycin cassette	R
5	GTGGCCGAGGAGCAGGACTGA	Phleomycin cassette	R

462 Orientation of primers: F, forward; R, reverse.

463 **Motility analyses**

464 *In silico* 2D tracking was performed as previously described [44]. For each BSF strain,
465 10 to 20 movies were recorded for 20 seconds (50 ms of exposure). Trypanosomes at
466 $1x10^6$ parasites/mL were maintained in matrix-dependent HMI-11 medium containing
467 0,5% methylcellulose at 37°C and were observed under the 10x objective of an
468 inverted DMI-4000B microscope (Leica) coupled to an ORCA-03G (Hamamatsu) or a
469 PRIME 95B (Photometrics) camera. Movies were converted with the MPEG Streamclip
470 V.1.9b3 software (Squared 5) and analyzed with the medeaLAB CASA Tracking V.5.5
471 software (medea AV GmbH). Results were analyzed as mean ± SD of three
472 independent experiments.

473 ***In vitro* bioluminescence quantification and analysis**

474 To perform the parasite density / bioluminescence intensity assay, BSF parasites were
475 counted, centrifuged, and resuspended in fresh HMI-11 medium. Then, 100 µL of this
476 suspension containing 10^6 parasites were transferred into black clear-bottom 96-well
477 plates and serial 2-fold dilutions were performed in triplicate adjusting the final volume
478 to 200 µL with 300 µg/mL of beetle luciferin (Promega, France). Luciferase activity was
479 quantified after 10 min of incubation with an IVIS Spectrum imager (PerkinElmer).
480 Imaging data analysis was performed with the Living Image 4.3.1 software
481 (PerkinElmer) by drawing regions of interest with constant size for well plate
482 quantification. Total photon flux was calculated after removal of intensity values from
483 WT parasites and / or parasite-free medium corresponding to the background noise.
484 Results were analyzed as mean ± SD of three independent experiments (Fig. S1 and
485 S3 A-B).

486 **Mouse infection and ethical statements**

487 Seven-week-old male BALB/c mice were purchased from Janvier Laboratory (sub-
488 strain BALB/cAnNRj) and used as models for experimental infection and monitoring of
489 the bioluminescence signal with the IVIS Spectrum imager (PerkinElmer). This study
490 was conducted in strict accordance with the recommendations from the Guide for the
491 Care and Use of Laboratory Animals of the European Union (European Directive
492 2010/63/UE) and the French Government. The protocol was approved by the "Comité
493 d'éthique en expérimentation animale de l'Institut Pasteur" CETEA 89 (Permit number:
494 2012-0043 and 2016-0017) and undertaken in compliance with the Institut Pasteur
495 Biosafety Committee (protocol CHSCT 12.131). BR is authorized to perform
496 experiments on vertebrate animals (license #A-75-2035) and is responsible for all the
497 experiments conducted personally or under his supervision. For *in vivo* infections,

498 groups of four and three animals (*FLAM8* knockdown and knockout-infected mice,
499 respectively) were injected intraperitoneally (IP) with 10^5 slender BSF parasites,
500 washed in TDB (Trypanosome Dilution Buffer: 5 mM KCl, 80 mM NaCl, 1 mM
501 $MgSO_4$*$7H_2O$, 20 mM Na_2HPO_4, 2 mM NaH_2PO_4, 20 mM glucose) and resuspended
502 in 100 µl of PBS prior animal inoculation.

503 ***In vivo* bioluminescence imaging (BLI) analyses**

504 Infection with bioluminescent parasites was monitored daily by detecting the
505 bioluminescence signal in whole animals with the IVIS Spectrum imager (PerkinElmer).
506 The equipment consists of a cooled charge-coupled camera mounted on a light-tight
507 chamber with a nose cone delivery device to keep the mice anaesthetized during
508 image acquisition with 1.5-2% isoflurane. A heated stage is comprised within the IVIS
509 Spectrum imager to maintain optimum body temperature. D-luciferin potassium salt
510 (Promega) stock solution was prepared in sterile PBS at 33.33 mg/mL and stored in a
511 -20°C freezer. To produce bioluminescence, mice were inoculated by the
512 intraperitoneal route (IP) with 150 µL of D-luciferin stock solution (250 mg/Kg body
513 weight). After 10 minutes of incubation to allow substrate dissemination, all mice were
514 anaesthetized in an oxygen-rich induction chamber with 1.5-2% isoflurane, and dorsal
515 and ventral BLI images were acquired by using automatic exposure (0.5 seconds to 5
516 minutes) depending on signal intensity.

517 Images were analyzed with the Living Image software version 4.3.1 (PerkinElmer).
518 Data were expressed in total photons/second (p/s) corresponding to the total flux of
519 bioluminescent signal according to the selected area (ventral and dorsal regions of
520 interest with constant size covering the total body of the mouse). The background noise
521 was removed by subtracting the bioluminescent signal of the control mouse from the
522 infected ones for each acquisition. For parasite dissemination analyses, a minimum

523 value of photons/second (p/s) was set for all animals in every time point to quantify the
524 exact dissemination area (in cm^2) over the whole animal body. Parasitemia was
525 determined daily following tail bleeds and assayed by automated fluorescent cell
526 counting with a Muse cytometer (Merck-Millipore, detection limit at 10^2 parasites/mL)
527 according to the manufacturer's recommendations. The quantification of the total
528 intravascular parasite population was assessed by calculating the blood volume of all
529 animals according to their body weight and referring to daily parasitemia.
530 To quantify the total number of parasites by BLI (intravascular plus extravascular
531 trypanosomes), an *in vivo* standard curve was performed (Fig. S3 C-D). Since the
532 bioluminescent emission of cultured parental, KO subclones and rescue parasites was
533 not significantly different (Fig. S3 A-B), the *in vivo* standard curve was obtained by
534 injecting IP increasing numbers (10^3, 10^4, 10^5, 10^6 and 10^7 parasites/animal) of
535 parental trypanosomes only (Fig. S3 C-D). After 2.5h, animals received 150 µL of D-
536 luciferin stock solution IP (250 mg/kg body weight), 10 minutes prior image acquisition.
537 During this time, mice were anaesthetized with 1.5-2% isoflurane, and images were
538 acquired in the IVIS Spectrum imager by using automatic exposure settings. A region
539 of interest with a constant size was used to correlate the number of injected parasites
540 with the whole-body BLI signal. Non-infected controls were imaged and the total BLI
541 values used to subtract the background signal or noise. The signals in photons/second
542 were used to construct a standard curve to further interpolate the total number of
543 trypanosomes present in each animal during the entire experimental infection period
544 (Fig. S3 D). Subsequently, to obtain the number of extravascular parasites, the
545 calculated total number of parasites present in the vascular system was subtracted
546 from the total number of trypanosomes per animal body, resulting in estimating the

547 total parasite population colonizing the extravascular compartments at a given time
548 point.

549 **Endothelial transmigration assay**

550 Single donor cryopreserved Primary Human Umbilical Vein Endothelial Cells
551 (HUVECs) were obtained from Promocell and maintained as per the manufacturer's
552 instructions in 75 cm^2 flasks at 37°C with 5% CO_2 in endothelial cell growth medium
553 (Promocell) with 100 U/mL penicillin, and 100 µg/mL streptomycin (Gibco). Cells were
554 passaged at 80-90% confluence by dissociation with 0.04% Trypsin-0.03% EDTA
555 (Promocell), split at 1:3-1:5 ratios, and maintained for up to six passages. Polyester
556 transwell inserts for 24 well plates with 3 µm pore size (Corning) were coated with 10
557 µg/mL bovine fibronectin (Promocell) for one hour, the excess removed, and 600 µL
558 pre-warmed endothelial cell growth medium added to the lower chamber (Fig 6A). The
559 upper chamber was seeded with $2x10^4$ HUVECs per insert in a volume of 100 µL
560 endothelial cell growth medium. Media was exchanged in the upper and lower chamber
561 every two days until monolayer confluence reached (approximately 6 days).
562 Confluence was confirmed by FITC-dextran permeability assay and crystal violet
563 staining of a sacrificed transwell. Briefly, 1 mg/mL FITC-70kDa dextran (Sigma-Aldrich)
564 in endothelial cell growth medium was added to the upper chamber, incubated for 20
565 minutes and leakage to the lower chamber measured on a Qubit 4 Fluorometer
566 (Invitrogen). Leakage of <1% of the FITC-dextran was observed at confluence.
567 Monolayer integrity was confirmed by brightfield imaging of a transwell insert stained
568 with crystal violet as per the manufacturer's instructions (Millipore). To perform the
569 trypanosome transmigration assays, the confluent transwells were exchanged into a
570 new 24 well plate containing pre-warmed assay media (endothelial cell growth medium
571 supplemented with 20% trypanosome growth media) for two hours prior to performing

572 the assay. Cultured trypanosomes were collected by centrifugation at 900×g for 5 min
573 and resuspended in assay media at $2x10^6$/mL. The media in the upper chamber was
574 replaced with 100 µL of assay media containing $2x10^5$ trypanosomes and incubated
575 overnight at 37ºC, 5% CO_2. Each cell line was tested in triplicate transwells. Unbiased
576 quantification of trypanosome transmigration was determined after 24 hours by
577 collecting the media from the upper and lower chambers and transferring 100 µL to 96
578 well plates for automated counting using a Guava Easycyte HT system with a green
579 laser and a custom counting protocol for tdTomato fluorescent trypanosomes. The cell
580 counts per ml were used to calculate the number of trypanosomes in each
581 compartment and proportion of transmigration into the lower chamber. Trypanosome
582 transmigration was compared between the FLAM8 mutant cell lines and the parental
583 reference cell line using the Generalised Linear Model function in R with a Gaussian
584 family function and proportion transmigration as the dependant variable. A probability
585 value of $p<0.05$ was considered significant.

586 ***Ex vivo* RT-qPCR of mouse tissues**

587 *Biological samples*. After four weeks of *in vivo* monitoring, parental-, KO- and rescue-
588 infected mice were euthanized by an overdose of an anesthetic/analgesic mixture of
589 ketamine and xylazine (100 mg/kg and 10 mg/kg, respectively). Terminal bleeding was
590 then performed through the inferior *vena cava*, and the collected blood was directly
591 transferred in 1 ml RNAlater (ThermoFisher Scientific), snap frozen in liquid nitrogen
592 for long-term preservation. Next, perfusion was initiated by injecting 0.9% NaCl (pre-
593 heated at 37°C), to completely remove the blood from the animal's body (both organs
594 and vasculature), thus ensuring that subsequent analyses would only contain tissue-
595 dwelling trypanosomes. Finally, spleen, lungs, kidney, gut, testis, liver and skin tissue
596 samples were preserved in 1 ml RNAlater, snap frozen and stored in liquid nitrogen.

597 *RNA isolation*. Total RNA from samples was isolated using the QIAzol Reagent
598 (Qiagen) according to the manufacturer's instructions. Frozen tissue samples were
599 weighed and processed on ice to prevent thawing. Briefly, 30 mg of tissue were added
600 to 700 µl of QIAzol lysis reagent, or 250 µl of blood in 550 µl of QIAzol lysis reagent,
601 and samples were homogenized using the Precellys® Evolution Homogenizer (Bertin,
602 USA) with 2.8 mm stainless steel beads for 2 cycles of 1 min at 5000 rpm each,
603 followed by 15 sec of resting between them. Homogenates were then incubated for 5
604 min at room temperature before the addition of 140 µl chloroform (0.2 volume of
605 starting QIAzol lysis reagent), thoroughly mixed by vortexing for 15 seconds, incubated
606 5 min at room temperature and centrifuged at 12,000×g, 4°C, 15 min. The aqueous
607 phase containing the RNA was subsequently mixed with 1.5 volumes of absolute
608 ethanol and transferred into a RNeasy Mini spin column (QIAGEN®) following the
609 manufacturer's recommendations. The concentration of each RNA sample was
610 measured by spectrophotometric analysis in a NanoDrop 2000c (ThermoFisher
611 Scientific). Finally, RNA quality was determined by capillary electrophoresis in a 2100
612 Bioanalyzer (Agilent). Extracted RNA was stored at -80 °C prior to RT-qPCR analyses.
613 *DNAse treatment and validation*. Extracted RNA samples were subjected to a second
614 DNase treatment using Invitrogen's DNA-*free* kit (Life Technologies) according to
615 manufacturer's protocol. DNase treatment confirmation was performed by running a
616 qPCR targeting the *Tubulin* locus as housekeeping gene control. The primer pair used
617 is as follows: forward (FW), 5'-ACTGGGCAAAGGGCCACTAC-3'; reverse (RV), 5'-
618 CTCCTTGCAGCACACATCGA-3', with an amplicon size of 105 bp. Reactions were
619 done in a volume of 20 µl containing: 1 µl of RNA template (17 ng), 10 µl of 2X GoTaq
620 qPCR Master Mix Buffer, 2 µl of both FW and RV primers (at 10X) and 5 µl of Nuclease-
621 Free Water. Amplification was accomplished in a QuantStudio™ 3 thermal cycler

622 (Applied Biosystems) using the following program: 2 min at 95°C; 40 cycles at 94°C
623 15 sec; 55°C 1 min; and final 30 sec at 60°C. The absence of residual DNA in the
624 DNAse-treated RNA samples was thus confirmed when no amplification was
625 observed. RNA samples were further employed for gene expression quantification.
626 *Primer design of target genes*. For *FLAM8* amplification, primers were designed to
627 recognize the 324-bp region suppressed during *FLAM8* knockout generation: FW, 5'-
628 GCATCGTTCGTGAGGTTGGA-3'; RV, 5'-GTTCCTCTTCGTCATCTGGTTCA-3'. The
629 amplicon size was 88 bp. For Protein Associated to Differentiation 1 (PAD1)
630 quantification in infected samples, primer sequences were described elsewhere
631 (Saldivia et al. 2016) and are listed below: FW, 5'-
632 TCATGGTTTCGCCATTCTCGTAACC-3'; RV, 5'-
633 CTCAGCCACTTCTCTCCTACAACAC-3'. Amplicon size is 156 bp.
634 *Real time RT-PCR assay*. One step RT-PCR kit (Promega) was used. Reactions were
635 prepared in a volume of 20 µl, containing: 1 µl of RNA template (17 ng), 10 µl of 2X
636 GoTaq qPCR Master Mix Buffer, 0.4 µl of 50X GoScript™ RT Mix for 1-Step RT-qPCR,
637 2 µl of both FW and RV primers (10X), and 4,6 µl of Nuclease-Free Water. Reverse
638 transcription and amplification were accomplished in one step in a QuantStudio™ 3
639 thermal cycler (Applied Biosystems) using the following incubation program: 15 min at
640 42°C; 10 min at 95°C; 40 cycles of 95°C during 30 sec; 55°C for *Tubulin*, 58°C for
641 *FLAM8* or 60°C for *PAD1* during 1 min; final 72°C during 30 sec. A melt curve program
642 was included: 15 sec at 95°C; 55°C for *Tubulin*, 58°C for *FLAM8* or 60°C for *PAD1*
643 during 1 min; 95°C for 10 sec. Amplicons were then analyzed by gel electrophoresis.
644 Negative and positive controls consisted of RNA extracted from uninfected mice and
645 cultured trypanosomes, respectively.
646 **Table 2.** Oligonucleotides used for *ex vivo* RT-qPCR of infected tissues.

Primer		Sequence	Purpose
Tubulin	F	ACTGGGCAAAGGGCCACTAC	Housekeeping control. Total trypanosome quantification (both SL and ST parasites) through standard curve generation.
	R	CTCCTTGCAGCACACATCGA	
FLAM8	F	GCATCGTTCGTGAGGTTGGA	Detection of parasites expressing *FLAM8*. The amplified sequence is absent in *FLAM8* KO mutants.
	R	GTTCCTCTTCGTCATCTGGTTCA	
PAD-1	F	TCATGGTTTCGCCATTCTCGTAACC	Quantification of transmissible ST parasites within *ex vivo* samples.
	R	CTCAGCCACTTCTCTCCTACAACAC	

647 Orientation of primers: F, forward; R, reverse.

648 *RT-qPCR data analysis*. All samples were amplified in triplicates and Cq mean values
649 were calculated. Considering that the same initial amounts of total mRNAs extracted
650 from each organ were used as RT-qPCR templates, the total number of parasites in
651 each sample was calculated for comparisons by using a *Tubulin* RT-qPCR standard
652 curve. Nine pools of cultured parasites (p) increasing by 10-folds from 10^1 to 10^8 were
653 extracted and tested in triplicates by *Tubulin* RT-qPCR to generate a standard curve.
654 The resulting standard curve's equation Cq = -2,87 x Log10(p) + 35,412 allowed us to
655 calculate the total number of parasites per sample according to the Cq values obtained
656 by *Tubulin* RT-qPCR on each sample. For normalization purposes, the difference
657 between the calculated number of parasites in each sample of a given mouse and the
658 calculated number of parasites in the blood sample from the same mouse (Delta
659 number of parasites) was calculated and plotted. *Tubulin* expression (CqTub) was also
660 used to normalize the *PAD1* mRNA levels (CqPAD1): the difference between the
661 CqPAD1 and the CqTub values was calculated for each organ of each mouse and
662 plotted as the Delta CqPAD1-CqTub. It allowed us to compare the relative proportions

663 of parasites expressing *PAD1* mRNAs between organs and strains, a higher Delta
664 CqPAD1-CqTub correlating with a lower amount of *PAD1* transcripts in the organ.

665 **Immunofluorescence analysis (IFA)**

666 Cultured parasites were washed twice in TDB and spread directly onto poly-L-lysine
667 coated slides. For methanol fixation, slides were air-dried for 10 min, fixed in methanol
668 at -20°C for 5 min and rehydrated for 20 min in PBS. For immunodetection, slides were
669 incubated for 1 h at 37°C with the appropriate dilution of the first antibody in 0.1% BSA
670 in PBS. After 3 consecutive 5 min washes in PBS, species and subclass-specific
671 secondary antibodies coupled to the appropriate fluorochrome (Alexa 488, Cy3, Cy5
672 Jackson ImmunoResearch) were diluted 1/400 in PBS containing 0.1% BSA and were
673 applied for 1 h at 37°C. After washing in PBS as indicated above, slides were finally
674 stained with 4',6-diamidino-2-phenylindole (DAPI, 1 µg/mL) for visualization of
675 kinetoplast and nuclear DNA content and mounted under cover slips with ProLong
676 antifade reagent (Invitrogen), as previously described [8]. Slides were observed under
677 an epifluorescence DMI4000 microscope (Leica) with a 100x objective (NA 1.4), an
678 EL6000 (Leica) as light excitation source and controlled by the Micro-Manager V1.4.22
679 software (NIH), and images were acquired using an ORCA-03G (Hamamatsu) or a
680 PRIME 95B (Photometrics) camera. Images were analyzed with ImageJ V1.8.0 (NIH).
681 The monoclonal antibody mAb25 (anti-mouse IgG2a, 1:10) was used as a flagellum
682 marker as it specifically recognizes the axoneme protein *Tb*SAXO1 [45]. FLAM8 was
683 detected using: i) a specific rabbit serum (1:500) kindly provided by Paul McKean
684 (University of Lancaster, UK), or ii) a monoclonal anti-mNeonGreen antibody (anti-
685 mouse IgG2c, 1:100, ChromoTek). CARP3 was detected using a polyclonal CARP3
686 antiserum (1:150) [21]. Stumpy BSF were identified at the molecular level with a rabbit
687 polyclonal anti-PAD1 antibody (kindly provided by Keith Matthews, University of

688 Edinburgh; dilution 1:300) [46]. In the case of RNAi knockdown experiments, IFA
689 signals were normalized using the signal obtained in non-induced controls as a
690 reference.

691 **Measurements, normalization, and statistical analyses**

692 Standardization of fluorescent signals was carried out by parallel setting of raw
693 integrated density signals in all the images to be compared in ImageJ V1.8.0 (NIH).
694 For clarity purposes, the brightness and contrast of several pictures were adjusted
695 after their analysis in accordance with editorial policies. Statistical analyses and plots
696 were performed with XLSTAT 2019.2.01 (Addinsoft) in Excel 2016 (Microsoft) or Prism
697 V9.3.1 (GraphPad). Statistical analyses include: (1) linear regression for
698 bioluminescence / fluorescence intensity vs. parasite density and RT-qPCR standard
699 curve, (2) two-sided ANOVA tests with Tukey or Dunnett's ad-hoc post-tests for inter-
700 group comparisons for growth curves and ΔCq comparisons of RT-qPCR data, all at
701 95% confidence.

702 **Acknowledgements**

703 We thank M. Bonhivers, D. Robinson, P. McKean, K. Matthews, and K. Gull for
704 providing various plasmids and antibodies. We gratefully acknowledge the UTechS
705 Photonic BioImaging (Imagopole), C2RT, Institut Pasteur, supported by the French
706 National Research Agency (France BioImaging; ANR-10–INSB–04; Investments for
707 the Future). We are grateful to P. Bastin for his strong scientific and human support.
708 We warmly thank M. Boshart, P. Bastin, and S. Bonnefoy for their critical reading of
709 the manuscript.

710 **Funding**

711 This work was supported by the Institut Pasteur, the French Government
712 Investissement d'Avenir programme - Laboratoire d'Excellence "Integrative Biology of
713 Emerging Infectious Diseases" (ANR-10-LABX-62-IBEID) and the French National
714 Agency for Scientific Research (projects ANR-14-CE14-0019-01 EnTrypa and ANR-
715 18-CE15-0012 TrypaDerm). AML and AnC are funded by a Wellcome Senior
716 Fellowship to AML (209511/Z/17/Z). None of these funding sources has a direct
717 scientific or editorial role in the present study.

718 **Author contributions**

719 ECA and BR designed the study. ECA, JMTN, CT, AnC and AlC performed the
720 experiments. ECA, JMTN, AnC and BR analyzed the data. ECA and BR wrote the
721 manuscript. ECA, AML and BR discussed the manuscript and acquired the funding.

722 **Competing interest**

723 All authors declare no financial relationships with any organizations that might have an
724 interest in the submitted work in the previous three years, no other relationships or

activities that could appear to have influenced the submitted work, and no other relationships or activities that could appear to have influenced the submitted work.

727 **Figure captions**

728

729 **Figure 1. Characterization of the *FLAM8::mNG FLAM8^{RNAi}* strain *in vitro* and *in***
730 ***vivo* functional investigation in the mammalian host. A)** Expression of *FLAM8*
731 mRNA assessed by RT-PCR by the comparative $\Delta\Delta C_T$ method in control, non-induced
732 and induced *FLAM8::mNG FLAM8^{RNAi}* parasites (72 h). **B)** Immunofluorescence
733 pictures of non-induced (upper panels) and induced (bottom panels) *FLAM8::mNG*
734 *FLAM8^{RNAi}* BSF during 72 h. Methanol-fixed trypanosomes were stained with an anti-
735 mNG antibody (green) and DAPI for DNA content (blue). The scale bars represent 5
736 µm. **C)** Growth curves of control, non-induced and induced *FLAM8::mNG FLAM8^{RNAi}*
737 BSF parasites. All cell lines received 1 µg tetracycline for 6 days. Control parasites are
738 Lister 427 "Single Marker" BSF parasites that do not bear the pZJM-FLAM8 plasmid
739 for RNAi silencing. Results represent the mean (± standard deviation, SD) of three
740 independent experiments. **D)** Groups of 4 BALB/c mice were injected IP with either
741 control, non-induced or induced *FLAM8^{RNAi}* BSF trypanosomes. One PBS-injected
742 BALB/c animal was used as negative control. Representative normalized *in vivo*
743 images of the bioluminescence radiance signal (in photons / second / cm^2 / steradian)
744 emitted from BALB/c mice infected with control, non-induced and induced
745 *FLAM8::mNG FLAM8^{RNAi}* parasites 4 days post-infection (non-infected technical
746 control mice were negative for bioluminescence, not shown). RNAi silencing of *FLAM8*
747 was maintained *in vivo* by the addition of doxycycline in sugared drinking water 48 h
748 prior infection and until the end of the experiment. **E)** Number of parasites in the blood
749 (intravascular, IV) of infected BALB/c mice during the course of the infection (5 days).
750 **F)** Number of parasites in the extravascular compartment (extravascular, EV) of the
751 same infected mice as in E). **G)** Dissemination of control, non-induced and induced

752 *FLAM8::mNG FLAM8*^{RNAi} parasites, measured over the entire animal body (in cm^2)
753 through the total bioluminescent surface, during the entire infection course. Results
754 represent means ± standard deviation (SD).
755
756 **Figure 2. Characterization of Δ*FLAM8* null mutants *in vitro*. A)**
757 Immunofluorescence pictures of parental, Δ*FLAM8* knockout and rescue pleomorphic
758 BSF parasites labelled with the anti-FLAM8 (green) and mAb25 (axoneme in magenta)
759 antibodies, DAPI staining for DNA content (blue). Scale bars show 5 µm. **B)** Growth
760 curve of one parental, three Δ*FLAM8* subclones and one rescue pleomorphic BSF
761 trypanosome cell lines over 6 consecutive days. **C)** Measurements of the flagellum
762 length based on the axonemal marker mAb25 profiles in parental, three Δ*FLAM8*
763 subclones and rescue parasites. No statistical differences were found. **D, E)** Motility
764 tracking analysis showing the average speeds (D) and linearity (E) of BSF cell lines in
765 matrix-dependent culture medium. No statistical differences were observed. The
766 number of parasites considered for quantifications (N) is indicated above graphs (C),
767 (D) and (E). Results represent the mean ± standard deviation (SD) of three
768 independent experiments. Statistical tests included one-way ANOVA and Tukey's ad-
769 hoc post-tests for multiple comparisons.
770
771 **Figure 3. Functional investigations on the Δ*FLAM8* null mutants *in vivo* in the**
772 **mammalian host.** Groups of 3 BALB/c mice were injected IP with either one parental,
773 three ΔF*LAM8* null subclones or one rescue strains. One PBS-injected BALB/c animal
774 was used as negative control. **A)** Normalized *in vivo* images of the bioluminescence
775 radiance intensity (in photons / second / cm^2 / steradian) emitted 8 days post-infection
776 in BALB/c mice infected with parental, three Δ*FLAM8* subclones or rescue parasites

777 (non-infected control mice C- were negative for bioluminescence). **B)** Total number of
778 parasites in the blood of infected mice (intravascular, IV) during the infection (4 weeks).
779 Statistically significant differences ($p<0.01$) are indicated with one, two or three
780 asterisks (*, **, ***) representing differences between the parental strain and one, two
781 or three Δ*FLAM8* subclones, respectively. **C)** Total number of extravascular (EV)
782 trypanosomes in the same mice. Statistically significant differences between the
783 parental strain and Δ*FLAM8* subclones are indicated as in B). **D)** Dissemination of the
784 parental, three Δ*FLAM8* subclones and rescue parasite strains, measured over the
785 entire animal body (in cm^2) through the total surface of bioluminescent signal, during
786 the entire infection course. Statistically significant differences between the parental
787 strain and Δ*FLAM8* subclones are indicated as described above. Results represent
788 means ± standard deviation (SD). Statistical tests included two-way ANOVA and
789 Tukey's ad-hoc post-tests for multiple comparisons.
790
791 **Figure 4. The absence of *FLAM8* reduces extravascular trypanosome**
792 **dissemination.** In a second experimental infection, groups of 3 BALB/c animals were
793 injected IP with either parental, three ΔF*LAM8* null subclones or rescue strains. One
794 PBS-injected BALB/c animal was used as negative control. **A)** Total number of
795 intravascular parasites (IV) during the infection period. **B)** Total number of
796 extravascular (EV) trypanosomes in the same mice. **C)** Dissemination of the parental,
797 three Δ*FLAM8* subclones and rescue parasite strains, measured over the entire animal
798 body (in cm^2) through the total surface of bioluminescent signal, during the entire
799 infection course. Statistically significant differences ($p<0.01$) are indicated with one or
800 three asterisks (*, ***) representing differences between the parental strain and one or
801 three Δ*FLAM8* subclones, respectively. **D)** Number of EV parasites per dissected

802 organ and strain obtained by RT-qPCR quantification according to normalized *Tubulin*
803 expression. **E)** Number of EV trypanosomes calculated as the average difference
804 between the number of parental, Δ*FLAM8* and rescue parasites in all organs vs.
805 intravascular trypanosomes by the RT-qPCR method. Statistical differences
806 ($p<0.0001$) according to one-way ANOVA and Dunnett's comparison tests.
807
808 **Figure 5. Parasite differentiation is not impacted in *FLAM8*-depleted**
809 **trypanosomes. A)** Representative immunofluorescence pictures of stumpy parasites
810 after *in vitro* differentiation from proliferative slenders of parental (left panel), three
811 Δ*FLAM8* subclones (middle panels) and rescue (right panel) parasite strains upon *in*
812 *vitro* treatment with a nucleotide 5'-AMP analog. Methanol-fixed parasites were
813 labelled with the anti-PAD-1 antibody (red), and DAPI staining for DNA content (blue).
814 Scale bars show 5 µm. **B)** Quantification of the proportion of stumpy trypanosomes in
815 all pleomorphic cell lines after *in vitro* differentiation. The number of parasites
816 considered for quantification (n) is indicated above the graph. No significant differences
817 were found (one-way ANOVA and Tukey's comparisons test). Results represent the
818 mean ± standard deviation (SD) of three independent experiments. **C)** Selected
819 immunofluorescence images of freshly *in vitro* differentiated procyclic cells.
820 Trypanosomes were doubly labelled with anti-FLAM8 (green) and mAb25 (axoneme
821 in magenta), DAPI staining showing DNA content in blue. Scale bars show 5 µm. **D)**
822 Upon differentiation, early procyclic forms (ePCF) of parental, three Δ*FLAM8*
823 subclones and rescue parasite strains were equally diluted, and their *in vitro* growth
824 assessed. Statistical differences ($p<0,01$) were observed only when comparing
825 parental and KO 2 ePCF trypanosomes (one-way ANOVA and Tukey's comparison
826 test). Results represent the mean ± standard deviation (SD) of four independent

827 experiments. **E)** Representative immunofluorescence images of naturally differentiated
828 stumpy trypanosomes from parental, one selected Δ*FLAM8* subclone and rescue
829 strains isolated from mouse blood during the first peak of parasitemia (first
830 experimental *in vivo* infection). Parasites were labelled with anti-PAD-1 antibody (red),
831 and DAPI staining for DNA content (blue). Scale bars show 5 µm. **F)** Relative
832 proportions of *PAD-1*-expressing parental, three Δ*FLAM8* subclones and rescue
833 strains by RT-qPCR on blood and dissected organs at day 23 of the second *in vivo*
834 challenge. *Tubulin* expression was used to normalize the *PAD-1* mRNA levels. **G)**
835 Average of whole-organism *PAD-1* expression referred to *Tubulin* normalization in
836 parental-, Δ*FLAM8*- and rescue-infected mice.
837
838 **Figure 6. Parasites lacking *FLAM8* are impaired in transmigrating through**
839 **endothelial cells *in vitro*. A)** Schematic representation of the trans-endothelial
840 migration assay, showing the transwell system (Boyden chamber) containing the upper
841 and the lower compartments, the monolayer of endothelial HUVEC cells and slender
842 trypanosomes seeded on the top of the chamber for 24 hours. **B)** After this period,
843 parasites within the upper and lower chambers were counted and values further used
844 to calculate the proportion of parental, three Δ*FLAM8* subclones and rescue parasites
845 that migrated through the endothelial monolayer into the lower compartment.
846 Trypanosome transmigration was compared between the FLAM8 mutant cell lines and
847 the parental reference line (100% of trans-endothelial migration) using the Generalised
848 Linear Model function in R with a Gaussian family function and proportion of
849 transmigration as the dependent variable. A probability value of $p<0.001$ was
850 considered significant (*). Error bars show SD. **C)** Representative immunofluorescence
851 images of cultured slender trypanosomes from parental, Δ*FLAM8* subclone and rescue

852 strains. Parasites were labelled with anti-CARP3 antibody (green intensity
853 normalized), and DAPI staining for DNA content (blue). Scale bars show 5 μm.

854 **Supporting information captions**

855

856 **Figure S1. Validation of the triple-reporter efficiency in monomorphic *FLAM8^{RNAi}***
857 **parasite lines.** Linear correlation between the number of parasites and the
858 bioluminescence (in p/s) emitted by monomorphic 427 *FLAM8::mNG FLAM8^{RNAi}* BSF
859 overexpressing the triple reporter chimeric protein [20], acquired by the IVIS Spectrum
860 imager. Parasites without the RNAi plasmid (control, C), non-treated with tetracycline
861 (non-induced, NI) and treated with tetracycline (induced, I) are shown. Representative
862 bioluminescent image of serial 1/2 dilutions performed in a 96-well plate (in photons /
863 second / cm^2 / steradian). RNAi induction was triggered by the addition of 1 µg
864 tetracycline and / or doxycycline for 72 h. Results represent the mean ± standard
865 deviation (SD) of three independent experiments.

866

867 **Figure S2. Molecular validation of the Δ*FLAM8* null mutant cell lines. A)** Whole-
868 genome sequencing results showing *FLAM8* wild-type allele (WT, upper panel), the
869 partial loss of the 5' *FLAM8* ORF in Δ*FLAM8* knockout trypanosomes (middle panel;
870 the black arrow is showing the absence of reads at the *FLAM8* 5' ORF in the knockout
871 line); and the restoration of the full *FLAM8* gene in rescue parasites (bottom panel; the
872 black arrow is showing the absence of reads within the *pac* cassette due to the
873 insertion of the new construct bearing the *ble* resistance marker), relative to the
874 number of reads per 100-nt read length. The presence of the correct antibiotic
875 cassettes is shown for knockout and rescue parasites (right middle and bottom panels).
876 Δ*FLAM8* knockout and rescue parasites also bear a construct for expression of a triple
877 reporter (TR) as assessed by the detection of *bsd* reads. **B)** Schemes showing the
878 structure of the *FLAM8* locus in wild-type parasites (upper scheme) and the integration

879 plan of the different cassettes for Δ*FLAM8* knockout (middle panel, *HYG*- and *PAC*-
880 containing schemes) and Rescue parasites (lower panel *HYG*- and *BLE*-containing
881 schemes). **C)** PCR confirmation of the successful integrations of all reporter cassettes.
882 Primer pairs used for PCRs are indicated at the bottom of each line and correspond to
883 those drawn on the schemes in B), along with the expected band sizes of the
884 corresponding diagnostic PCR. BSD: blasticidin; HYG: hygromycin; PAC: puromycin;
885 BLE: phleomycin.
886
887 **Figure S3. *In vitro* and *in vivo* validation of the triple-reporter efficiency in**
888 **pleomorphic Δ*FLAM8* mutant cell lines. A)** Representative bioluminescent image
889 (in photons / second) of serial 1/2 dilutions performed in a 96-well plate of pleomorphic
890 parental, Δ*FLAM8* knockout subclones and rescue parasites overexpressing the triple
891 reporter chimeric protein [20]. **B)** Linear correlation between the number of parasites
892 and the emitted bioluminescence (in photons / second) acquired by the IVIS Spectrum
893 imager. Results represent the mean ± standard deviation (SD) of three independent
894 experiments. **C)** Representative ventral view images of mice infected with increasing
895 amounts of parental trypanosomes (10^3, 10^4, 10^5, 10^6 and 10^7 parasites/animal)
896 acquired with the IVIS Spectrum imager 2.5 hours after IP injection. **D)** *In vivo* standard
897 curve showing the correlation between the number of injected parasites and the
898 bioluminescent signal (in photons/second, $R^2 = 1$). The standard curve was further
899 employed to calculate the total number of parasites present in infected animals through
900 whole-body BLI signal.
901
902

903 **References**

904 1. MacGregor P, Szoor B, Savill NJ, Matthews KR. Trypanosomal immune
905 evasion, chronicity and transmission: an elegant balancing act. Nat Rev Microbiol.
906 2012;10(6):431-8. Epub 2012/05/01. doi: 10.1038/nrmicro2779. PubMed PMID:
907 22543519.

908 2. Smith TK, Bringaud F, Nolan DP, Figueiredo LM. Metabolic reprogramming
909 during the *Trypanosoma brucei* life cycle. F1000Res. 2017;6. Epub 2017/06/20. doi:
910 10.12688/f1000research.10342.2. PubMed PMID: 28620452; PubMed Central
911 PMCID: PMCPMC5461901.

912 3. Rotureau B, Van Den Abbeele J. Through the dark continent: African
913 trypanosome development in the tsetse fly. Frontiers in cellular and infection
914 microbiology. 2013;3:53. Epub 2013/09/26. doi: 10.3389/fcimb.2013.00053. PubMed
915 PMID: 24066283; PubMed Central PMCID: PMC3776139.

916 4. Capewell P, Cren-Travaille C, Marchesi F, Johnston P, Clucas C, Benson RA,
917 et al. The skin is a significant but overlooked anatomical reservoir for vector-borne
918 African trypanosomes. eLife. 2016;5. doi: 10.7554/eLife.17716. PubMed PMID:
919 27653219; PubMed Central PMCID: PMCPMC5065312.

920 5. Caljon G, Van Reet N, De Trez C, Vermeersch M, Perez-Morga D, Van Den
921 Abbeele J. The Dermis as a Delivery Site of *Trypanosoma brucei* for Tsetse Flies.
922 PLoS Pathog. 2016;12(7):e1005744. doi: 10.1371/journal.ppat.1005744. PubMed
923 PMID: 27441553; PubMed Central PMCID: PMCPMC4956260.

924 6. Trindade S, Rijo-Ferreira F, Carvalho T, Pinto-Neves D, Guegan F, Aresta-
925 Branco F, et al. *Trypanosoma brucei* Parasites Occupy and Functionally Adapt to the
926 Adipose Tissue in Mice. Cell Host Microbe. 2016. doi: 10.1016/j.chom.2016.05.002.
927 PubMed PMID: 27237364.

928 7. Crilly NP, Mugnier MR. Thinking outside the blood: Perspectives on tissue-
929 resident *Trypanosoma brucei*. PLoS Pathog. 2021;17(9):e1009866. Epub 2021/09/17.
930 doi: 10.1371/journal.ppat.1009866. PubMed PMID: 34529724; PubMed Central
931 PMCID: PMCPMC8445408.
932 8. Rotureau B, Subota I, Bastin P. Molecular bases of cytoskeleton plasticity during
933 the *Trypanosoma brucei* parasite cycle. Cell Microbiol. 2011;13(5):705-16. Epub
934 2010/12/17. doi: 10.1111/j.1462-5822.2010.01566.x. PubMed PMID: 21159115.
935 9. Broadhead R, Dawe HR, Farr H, Griffiths S, Hart SR, Portman N, et al. Flagellar
936 motility is required for the viability of the bloodstream trypanosome. Nature.
937 2006;440(7081):224-7. Epub 2006/03/10. doi: nature04541 [pii]
938 10.1038/nature04541. PubMed PMID: 16525475.
939 10. Kohl L, Robinson D, Bastin P. Novel roles for the flagellum in cell
940 morphogenesis and cytokinesis of trypanosomes. EMBO J. 2003;22(20):5336-46.
941 Epub 2003/10/09. doi: 10.1093/emboj/cdg518. PubMed PMID: 14532107.
942 11. Tetley L, Vickerman K. Differentiation in *Trypanosoma brucei*: host-parasite cell
943 junctions and their persistence during acquisition of the variable antigen coat. J Cell
944 Sci. 1985;74:1-19. Epub 1985/03/01. PubMed PMID: 4030903.
945 12. Langousis G, Hill KL. Motility and more: the flagellum of *Trypanosoma brucei*.
946 Nat Rev Microbiol. 2014;12(7):505-18. Epub 2014/06/17. doi: 10.1038/nrmicro3274.
947 PubMed PMID: 24931043.
948 13. Rotureau B, Morales MA, Bastin P, Spath GF. The flagellum-MAP kinase
949 connection in Trypanosomatids: a key sensory role in parasite signaling and
950 development? Cell Microbiol. 2009;11(5):710-18. Epub 2009/02/12. doi: CMI1295 [pii]
951 10.1111/j.1462-5822.2009.01295.x. PubMed PMID: 19207727.

952 14. Roditi I, Schumann G, Naguleswaran A. Environmental sensing by African
953 trypanosomes. Curr Opin Microbiol. 2016;32:26-30. Epub 2016/05/01. doi:
954 10.1016/j.mib.2016.04.011. PubMed PMID: 27131101.
955 15. Shimogawa MM, Ray SS, Kisalu N, Zhang Y, Geng Q, Ozcan A, et al. Parasite
956 motility is critical for virulence of African trypanosomes. Sci Rep. 2018;8(1):9122. Epub
957 2018/06/16. doi: 10.1038/s41598-018-27228-0. PubMed PMID: 29904094; PubMed
958 Central PMCID: PMCPMC6002391.
959 16. Subota I, Julkowska D, Vincensini L, Reeg N, Buisson J, Blisnick T, et al.
960 Proteomic analysis of intact flagella of procyclic *Trypanosoma brucei* cells identifies
961 novel flagellar proteins with unique sub-localisation and dynamics. Molecular & cellular
962 proteomics : MCP. 2014. Epub 2014/04/18. doi: 10.1074/mcp.M113.033357. PubMed
963 PMID: 24741115.
964 17. Fort C, Bonnefoy S, Kohl L, Bastin P. Intraflagellar transport is required for the
965 maintenance of the trypanosome flagellum composition but not its length. J Cell Sci.
966 2016;129(15):3026-41. Epub 2016/06/28. doi: 10.1242/jcs.188227. PubMed PMID:
967 27343245.
968 18. Bertiaux E, Morga B, Blisnick T, Rotureau B, Bastin P. A Grow-and-Lock Model
969 for the Control of Flagellum Length in Trypanosomes. Curr Biol. 2018. Epub
970 2018/11/20. doi: 10.1016/j.cub.2018.10.031. PubMed PMID: 30449671.
971 19. Calvo-Alvarez E, Bonnefoy S, Salles A, Benson FE, McKean PG, Bastin P, et
972 al. Redistribution of FLAgellar Member 8 during the trypanosome life cycle:
973 Consequences for cell fate prediction. Cell Microbiol. 2021;23(9):e13347. Epub
974 2021/04/26. doi: 10.1111/cmi.13347. PubMed PMID: 33896083; PubMed Central
975 PMCID: PMCPMC8459223.

976 20. Calvo-Alvarez E, Cren-Travaille C, Crouzols A, Rotureau B. A new chimeric
977 triple reporter fusion protein as a tool for *in vitro* and *in vivo* multimodal imaging to
978 monitor the development of African trypanosomes and *Leishmania* parasites. Infect
979 Genet Evol. 2018. Epub 2018/01/18. doi: 10.1016/j.meegid.2018.01.011. PubMed
980 PMID: 29339220.
981 21. Bachmaier S, Giacomelli G, Calvo-Alvarez E, Vieira LR, Van Den Abbeele J,
982 Aristodemou A, et al. A multi-adenylate cyclase regulator at the flagellar tip controls
983 African trypanosome transmission. Nat Commun. 2022;13(1):5445. Epub 2022/09/17.
984 doi: 10.1038/s41467-022-33108-z. PubMed PMID: 36114198; PubMed Central
985 PMCID: PMCPMC9481589.
986 22. Rojas F, Silvester E, Young J, Milne R, Tettey M, Houston DR, et al.
987 Oligopeptide Signaling through TbGPR89 Drives Trypanosome Quorum Sensing. Cell.
988 2018. Epub 2018/12/07. doi: 10.1016/j.cell.2018.10.041. PubMed PMID: 30503212.
989 23. Goodwin LG. The pathology of African trypanosomiasis. Trans R Soc Trop Med
990 Hyg. 1970;64(6):797-817. Epub 1970/01/01. PubMed PMID: 5495630.
991 24. Biteau N, Asencio C, Izotte J, Rousseau B, Fevre M, Pillay D, et al.
992 *Trypanosoma brucei gambiense* Infections in Mice Lead to Tropism to the
993 Reproductive Organs, and Horizontal and Vertical Transmission. PLoS Negl Trop Dis.
994 2016;10(1):e0004350. Epub 2016/01/07. doi: 10.1371/journal.pntd.0004350. PubMed
995 PMID: 26735855; PubMed Central PMCID: PMCPMC4703293.
996 25. Carvalho T, Trindade S, Pimenta S, Santos AB, Rijo-Ferreira F, Figueiredo LM.
997 *Trypanosoma brucei* triggers a marked immune response in male reproductive organs.
998 PLoS Negl Trop Dis. 2018;12(8):e0006690. Epub 2018/08/16. doi:
999 10.1371/journal.pntd.0006690. PubMed PMID: 30110342; PubMed Central PMCID:
1000 PMCPMC6093638.

1001 26. Caljon G, Van Den Abbeele J, Sternberg JM, Coosemans M, De Baetselier P,
1002 Magez S. Tsetse fly saliva biases the immune response to Th2 and induces anti-vector
1003 antibodies that are a useful tool for exposure assessment. Int J Parasitol.
1004 2006;36(9):1025-35. Epub 2006/06/17. doi: 10.1016/j.ijpara.2006.05.002. PubMed
1005 PMID: 16777113.
1006 27. Camara M, Soumah AM, Ilboudo H, Travaille C, Clucas C, Cooper A, et al.
1007 Extravascular Dermal Trypanosomes in Suspected and Confirmed Cases of
1008 *gambiense* Human African Trypanosomiasis. Clin Infect Dis. 2021;73(1):12-20. Epub
1009 2020/07/09. doi: 10.1093/cid/ciaa897. PubMed PMID: 32638003; PubMed Central
1010 PMCID: PMCPMC8246823.
1011 28. Bargul JL, Jung J, McOdimba FA, Omogo CO, Adung'a VO, Kruger T, et al.
1012 Species-Specific Adaptations of Trypanosome Morphology and Motility to the
1013 Mammalian Host. PLoS Pathog. 2016;12(2):e1005448. Epub 2016/02/13. doi:
1014 10.1371/journal.ppat.1005448. PubMed PMID: 26871910; PubMed Central PMCID:
1015 PMCPMC4752354.
1016 29. Sun SY, Kaelber JT, Chen M, Dong X, Nematbakhsh Y, Shi J, et al. Flagellum
1017 couples cell shape to motility in *Trypanosoma brucei*. Proc Natl Acad Sci U S A.
1018 2018;115(26):E5916-E25. Epub 2018/06/13. doi: 10.1073/pnas.1722618115. PubMed
1019 PMID: 29891682; PubMed Central PMCID: PMCPMC6042131.
1020 30. De Niz M, Bras D, Ouarne M, Pedro M, Nascimento AM, Henao Misikova L, et
1021 al. Organotypic endothelial adhesion molecules are key for *Trypanosoma brucei*
1022 tropism and virulence. Cell Rep. 2021;36(12):109741. Epub 2021/09/23. doi:
1023 10.1016/j.celrep.2021.109741. PubMed PMID: 34551286; PubMed Central PMCID:
1024 PMCPMC8480282.

1025 31. Shaw S, DeMarco SF, Rehmann R, Wenzler T, Florini F, Roditi I, et al. Flagellar
1026 cAMP signaling controls trypanosome progression through host tissues. Nat Commun.
1027 2019;10(1):803. Epub 2019/02/20. doi: 10.1038/s41467-019-08696-y. PubMed PMID:
1028 30778051; PubMed Central PMCID: PMCPMC6379439.
1029 32. Shaw S, Knusel S, Abbuhl D, Naguleswaran A, Etzensperger R, Benninger M,
1030 et al. Cyclic AMP signalling and glucose metabolism mediate pH taxis by African
1031 trypanosomes. Nat Commun. 2022;13(1):603. Epub 2022/02/03. doi: 10.1038/s41467-
1032 022-28293-w. PubMed PMID: 35105902; PubMed Central PMCID:
1033 PMCPMC8807625.
1034 33. Le Ray D, Barry JD, Easton C, Vickerman K. First tsetse fly transmission of the
1035 "AnTat" serodeme of *Trypanosoma brucei*. Ann Soc Belg Med Trop. 1977;57(4-5):369-
1036 81. Epub 1977/01/01. PubMed PMID: 610616.
1037 34. Bohringer S, Hecker H. Quantitative ultrastructural differences between strains
1038 of the *Tryponasoma brucei* subgroup during transformation in blood. J Protozool.
1039 1974;21(5):694-8. Epub 1974/11/01. doi: 10.1111/j.1550-7408.1974.tb03731.x.
1040 PubMed PMID: 4449091.
1041 35. Hirumi H, Hirumi K. Continuous cultivation of *Trypanosoma brucei* blood stream
1042 forms in a medium containing a low concentration of serum protein without feeder cell
1043 layers. J Parasitol. 1989;75(6):985-9. Epub 1989/12/01. PubMed PMID: 2614608.
1044 36. Barquilla A, Saldivia M, Diaz R, Bart JM, Vidal I, Calvo E, et al. Third target of
1045 rapamycin complex negatively regulates development of quiescence in *Trypanosoma*
1046 *brucei*. Proc Natl Acad Sci U S A. 2012;109(36):14399-404. doi:
1047 10.1073/pnas.1210465109. PubMed PMID: 22908264; PubMed Central PMCID:
1048 PMCPMC3437835.

1049 37. Czichos J, Nonnengaesser C, Overath P. *Trypanosoma brucei*: cis-aconitate
1050 and temperature reduction as triggers of synchronous transformation of bloodstream
1051 to procyclic trypomastigotes in vitro. Exp Parasitol. 1986;62(2):283-91. Epub
1052 1986/10/01. doi: 10.1016/0014-4894(86)90033-0. PubMed PMID: 3743718.
1053 38. Doyle JJ, Hirumi H, Hirumi K, Lupton EN, Cross GA. Antigenic variation in
1054 clones of animal-infective *Trypanosoma brucei* derived and maintained in vitro.
1055 Parasitology. 1980;80(2):359-69. Epub 1980/04/01. doi:
1056 10.1017/s0031182000000810. PubMed PMID: 6102753.
1057 39. Wang Z, Morris JC, Drew ME, Englund PT. Inhibition of *Trypanosoma brucei*
1058 gene expression by RNA interference using an integratable vector with opposing T7
1059 promoters. J Biol Chem. 2000;275(51):40174-9. Epub 2000/10/03. doi:
1060 10.1074/jbc.M008405200. PubMed PMID: 11013266.
1061 40. Wirtz E, Leal S, Ochatt C, Cross GA. A tightly regulated inducible expression
1062 system for conditional gene knock-outs and dominant-negative genetics in
1063 *Trypanosoma brucei*. Mol Biochem Parasitol. 1999;99(1):89-101. Epub 1999/04/24.
1064 PubMed PMID: 10215027.
1065 41. Redmond S, Vadivelu J, Field MC. RNAit: an automated web-based tool for the
1066 selection of RNAi targets in *Trypanosoma brucei*. Mol Biochem Parasitol.
1067 2003;128(1):115-8. Epub 2003/04/23. doi: 10.1016/s0166-6851(03)00045-8. PubMed
1068 PMID: 12706807.
1069 42. Burkard G, Fragoso CM, Roditi I. Highly efficient stable transformation of
1070 bloodstream forms of *Trypanosoma brucei*. Mol Biochem Parasitol. 2007;153(2):220-
1071 3. Epub 2007/04/06. doi: 10.1016/j.molbiopara.2007.02.008. PubMed PMID:
1072 17408766.

1073 43. Kelly S, Reed J, Kramer S, Ellis L, Webb H, Sunter J, et al. Functional genomics
1074 in *Trypanosoma brucei*: a collection of vectors for the expression of tagged proteins
1075 from endogenous and ectopic gene loci. Mol Biochem Parasitol. 2007;154(1):103-9.
1076 Epub 2007/05/22. doi: S0166-6851(07)00099-0 [pii]
1077 10.1016/j.molbiopara.2007.03.012. PubMed PMID: 17512617.
1078 44. Rotureau B, Ooi CP, Huet D, Perrot S, Bastin P. Forward motility is essential for
1079 trypanosome infection in the tsetse fly. Cell Microbiol. 2014;16(3):425-33. Epub
1080 2013/10/19. doi: 10.1111/cmi.12230. PubMed PMID: 24134537.
1081 45. Dacheux D, Landrein N, Thonnus M, Gilbert G, Sahin A, Wodrich H, et al. A
1082 MAP6-related protein is present in protozoa and is involved in flagellum motility. PLoS
1083 One. 2012;7(2):e31344. Epub 2012/02/23. doi: 10.1371/journal.pone.0031344.
1084 PubMed PMID: 22355359; PubMed Central PMCID: PMCPMC3280300.
1085 46. Dean S, Marchetti R, Kirk K, Matthews KR. A surface transporter family conveys
1086 the trypanosome differentiation signal. Nature. 2009;459(7244):213-7. Epub
1087 2009/05/16. doi: nature07997 [pii]
1088 10.1038/nature07997. PubMed PMID: 19444208.
1089

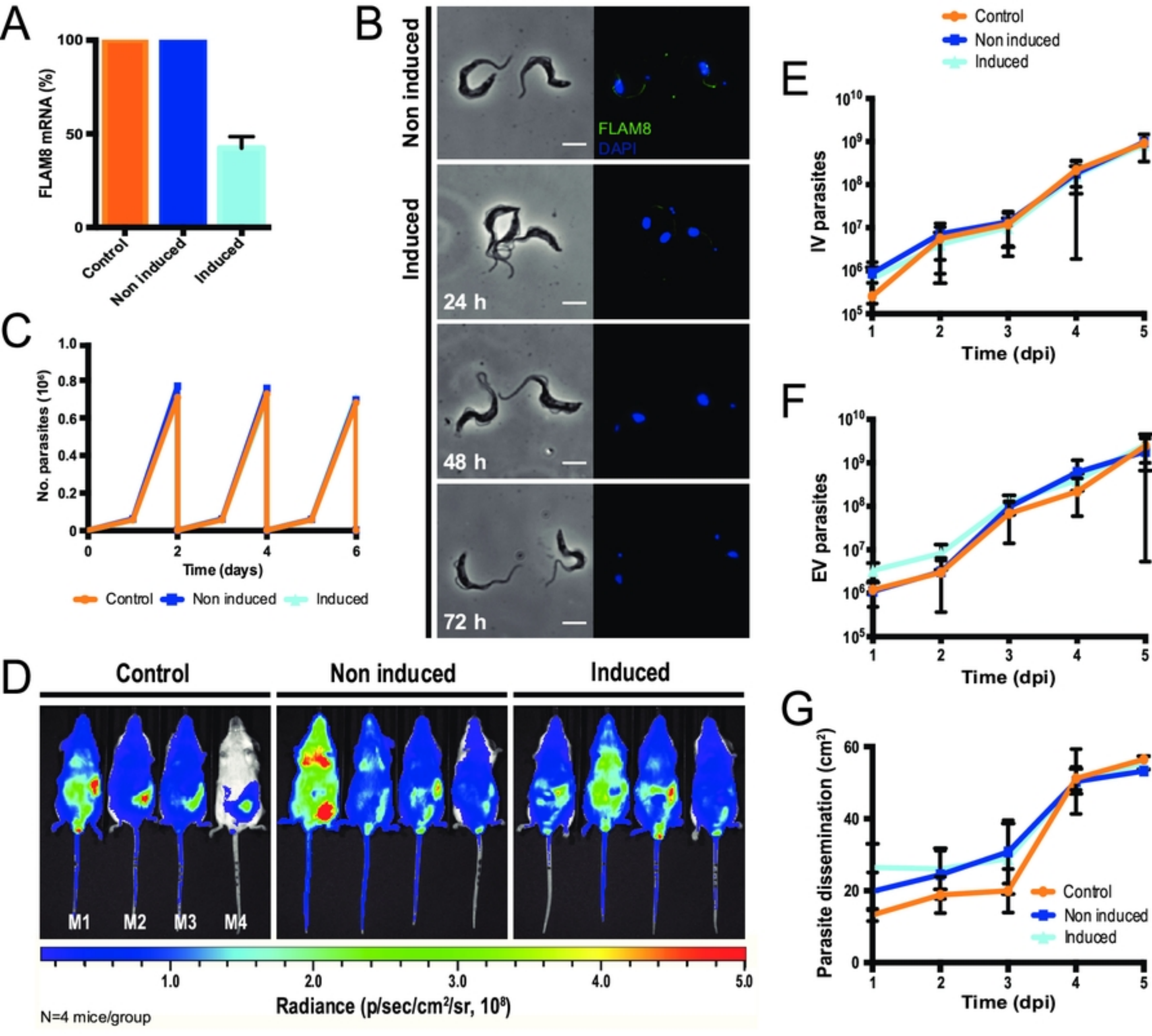
A
FLAM8 mRNA (%)
100
50
0
Control
Non induced
Induced
B
Non induced
Induced
FLAM8
DAPI
24 h
48 h
72 h
C
No. parasites (10⁶)
1.0
0.8
0.6
0.4
0.2
0
0
2
4
6
Time (days)
Control
Non induced
Induced
D
Control
Non induced
Induced
M1
M2
M3
M4
1.0
2.0
3.0
4.0
5.0
Radiance (p/sec/cm²/sr, 10⁸)
N=4 mice/group
E
Control
Non induced
Induced
IV parasites
10¹⁰
10⁹
10⁸
10⁷
10⁶
10⁵
1
2
3
4
5
Time (dpi)
F
EV parasites
10¹⁰
10⁹
10⁸
10⁷
10⁶
10⁵
1
2
3
4
5
Time (dpi)
G
Parasite dissemination (cm²)
60
40
20
0
1
2
3
4
5
Time (dpi)
Control
Non induced
Induced

Fig1

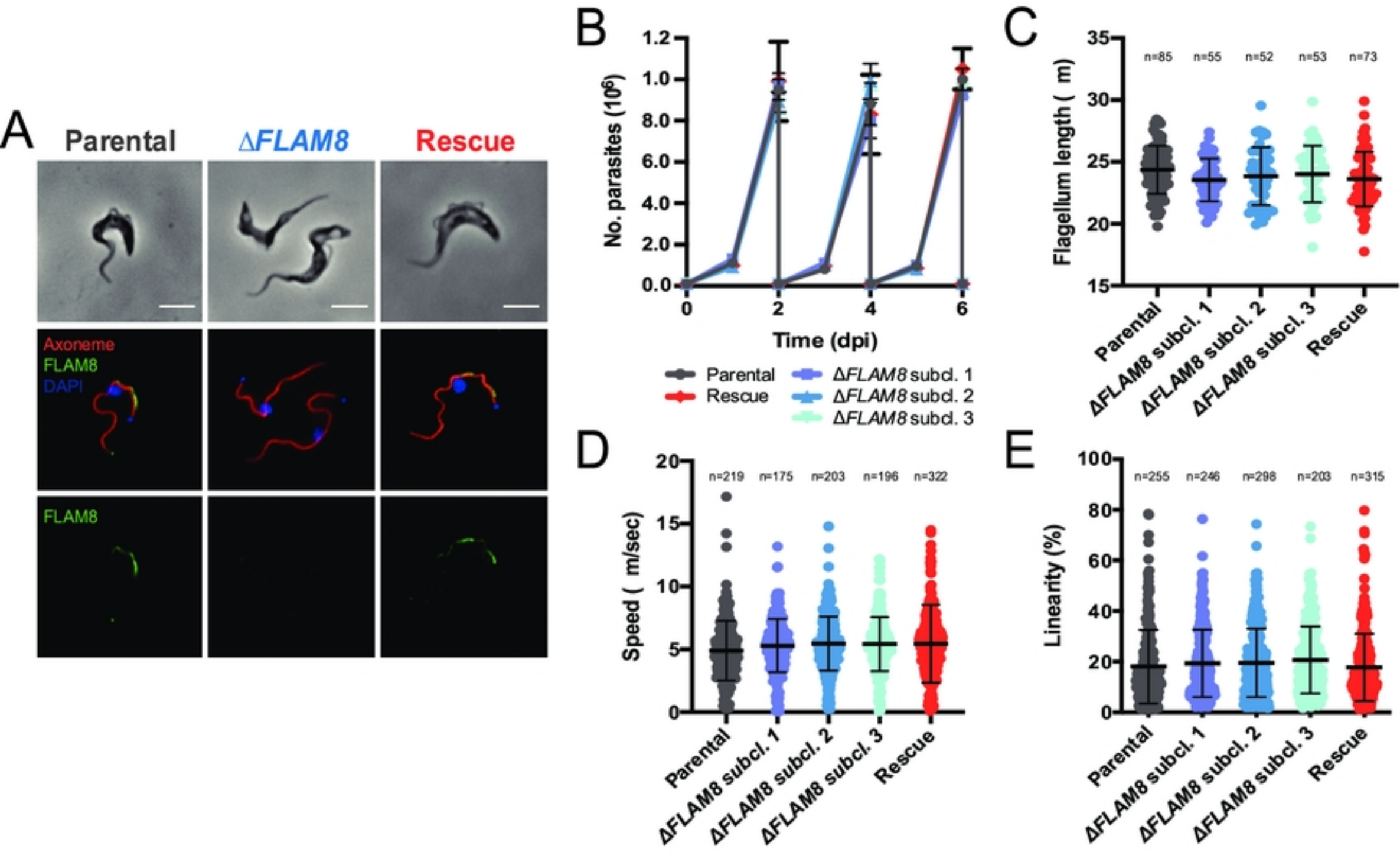
A
Parental
ΔFLAM8
Rescue
Axoneme
FLAM8
DAPI
FLAM8
B
No. parasites (10^6)
Time (dpi)
Parental
Rescue
ΔFLAM8 subcl. 1
ΔFLAM8 subcl. 2
ΔFLAM8 subcl. 3
C
Flagellum length (m)
n=85
n=55
n=52
n=53
n=73
Parental
ΔFLAM8 subcl. 1
ΔFLAM8 subcl. 2
ΔFLAM8 subcl. 3
Rescue
D
Speed (m/sec)
n=219
n=175
n=203
n=196
n=322
Parental
ΔFLAM8 subcl. 1
ΔFLAM8 subcl. 2
ΔFLAM8 subcl. 3
Rescue
E
Linearity (%)
n=255
n=246
n=298
n=203
n=315
Parental
ΔFLAM8 subcl. 1
ΔFLAM8 subcl. 2
ΔFLAM8 subcl. 3
Rescue

Fig2

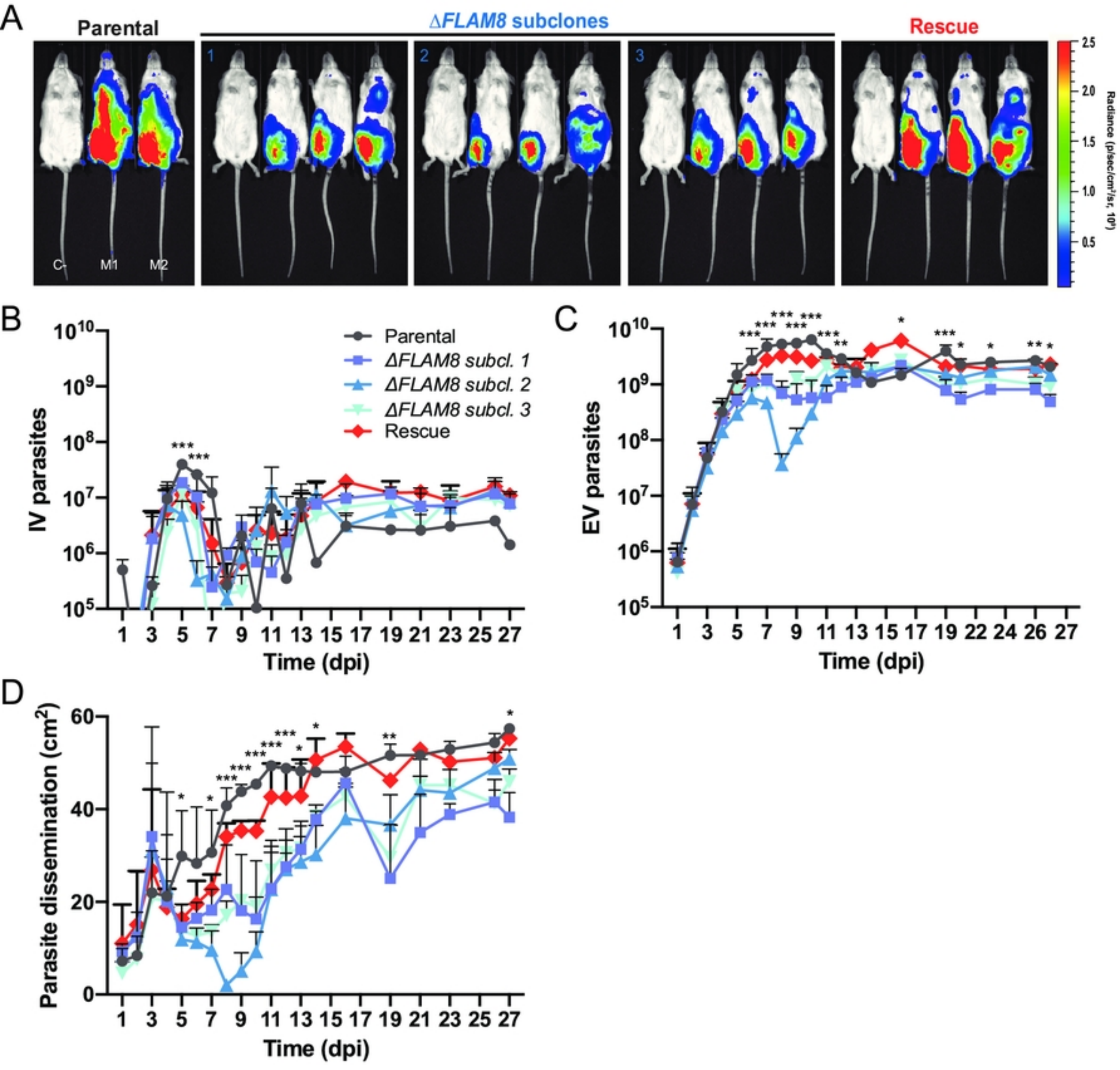
A
Parental
ΔFLAM8 subclones
Rescue
1
2
3
C-
M1
M2
Radiance (p/sec/cm²/sr, 10⁶)
B
IV parasites
Time (dpi)
Parental
ΔFLAM8 subcl. 1
ΔFLAM8 subcl. 2
ΔFLAM8 subcl. 3
Rescue
C
EV parasites
Time (dpi)
D
Parasite dissemination (cm²)
Time (dpi)

Fig3

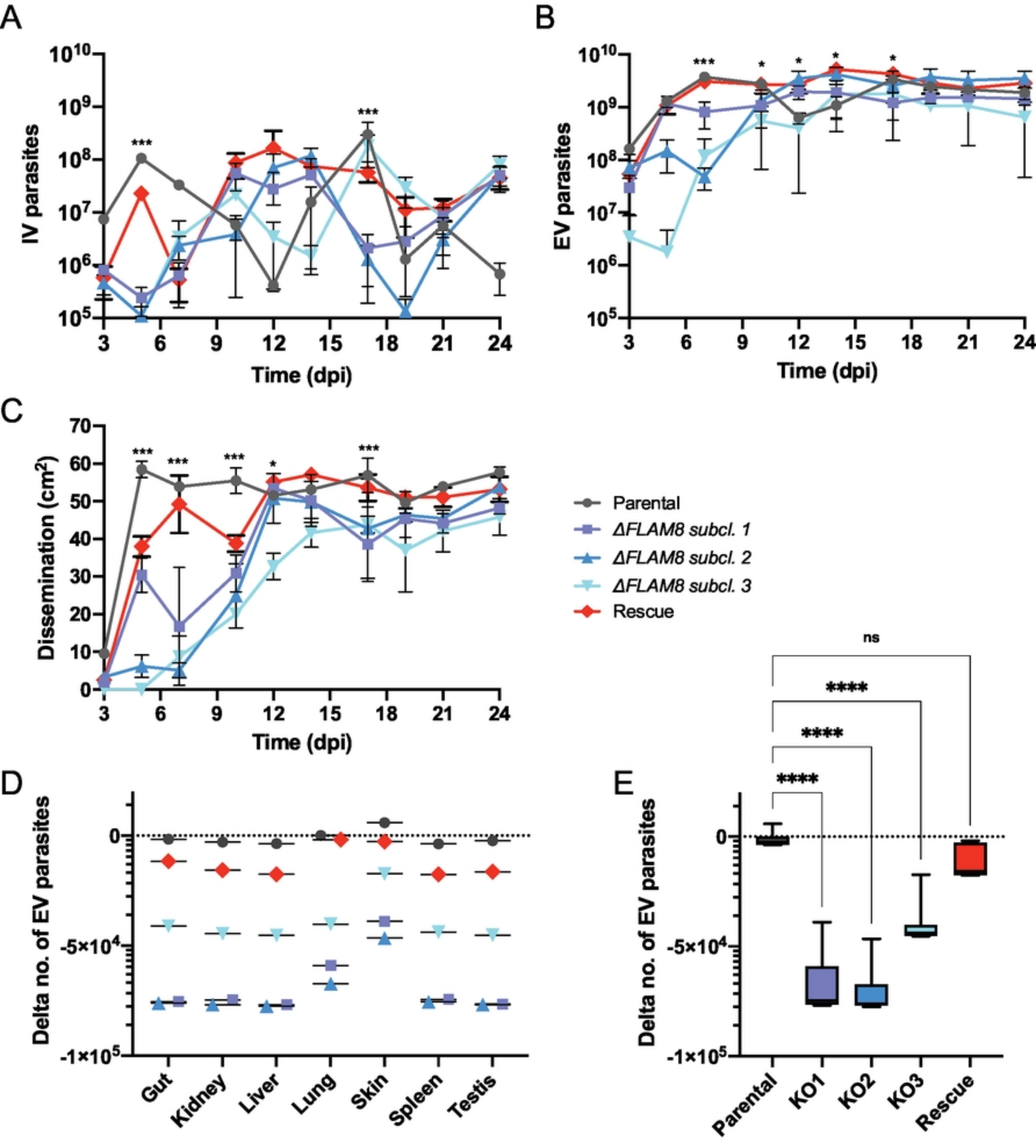
A
IV parasites
Time (dpi)
B
EV parasites
Time (dpi)
C
Dissemination (cm²)
Time (dpi)
Parental
ΔFLAM8 subcl. 1
ΔFLAM8 subcl. 2
ΔFLAM8 subcl. 3
Rescue
D
Delta no. of EV parasites
Gut
Kidney
Liver
Lung
Skin
Spleen
Testis
E
Delta no. of EV parasites
ns
****
****
****
Parental
KO1
KO2
KO3
Rescue

Fig4

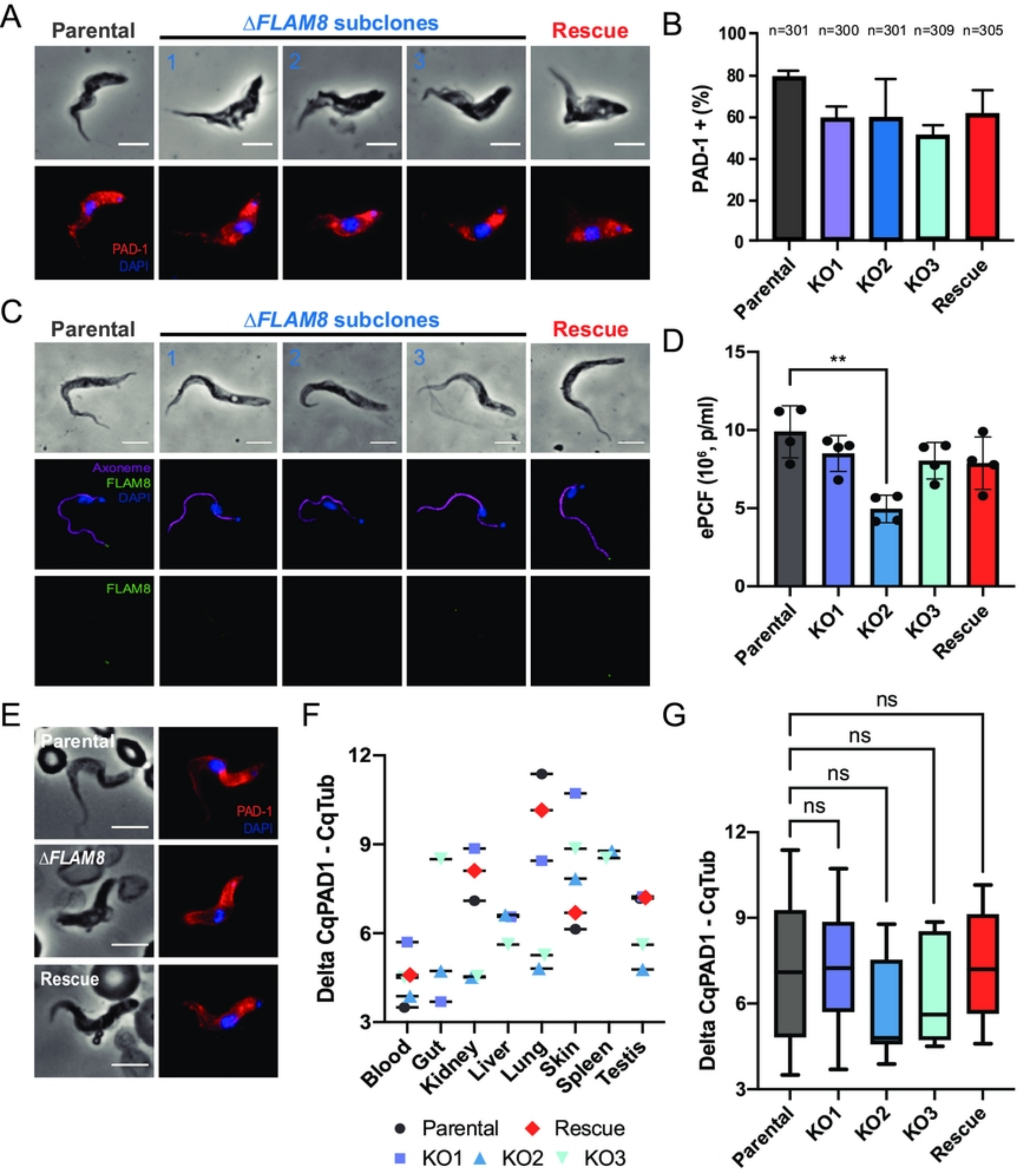
A
Parental
ΔFLAM8 subclones
Rescue
1
2
3
PAD-1
DAPI
B
n=301 n=300 n=301 n=309 n=305
PAD-1 + (%)
100
80
60
40
20
0
Parental
KO1
KO2
KO3
Rescue
C
Parental
ΔFLAM8 subclones
Rescue
1
2
3
Axoneme
FLAM8
DAPI
FLAM8
D
**
ePCF (10⁶, p/ml)
15
10
5
0
Parental
KO1
KO2
KO3
Rescue
E
Parental
PAD-1
DAPI
ΔFLAM8
Rescue
F
Delta CqPAD1 - CqTub
12
9
6
3
Blood
Gut
Kidney
Liver
Lung
Skin
Spleen
Testis
Parental
Rescue
KO1
KO2
KO3
G
ns
ns
ns
ns
Delta CqPAD1 - CqTub
12
9
6
3
Parental
KO1
KO2
KO3
Rescue

Fig5

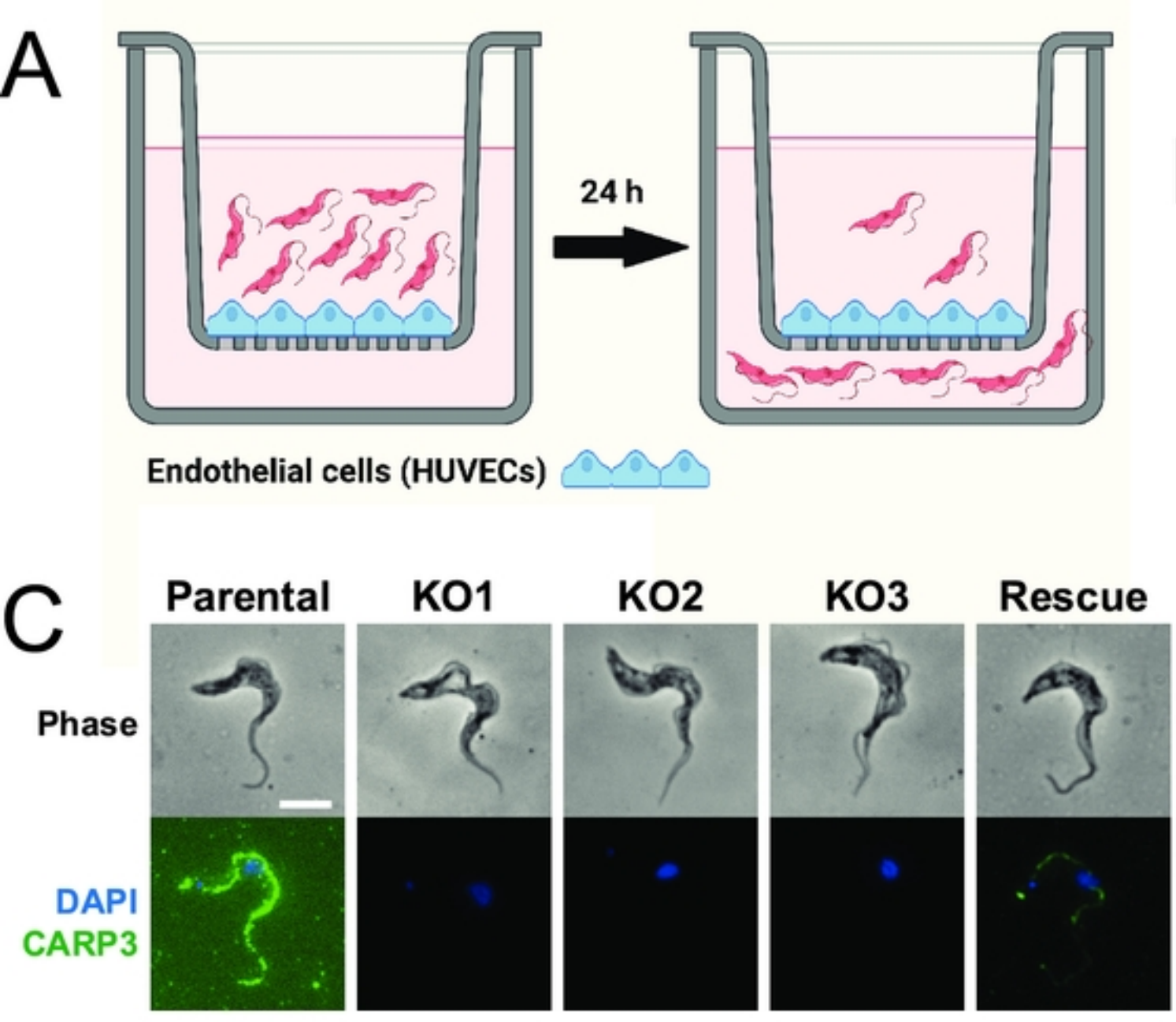
A
24 h
Endothelial cells (HUVECs)
C
Parental
KO1
KO2
KO3
Rescue
Phase
DAPI
CARP3

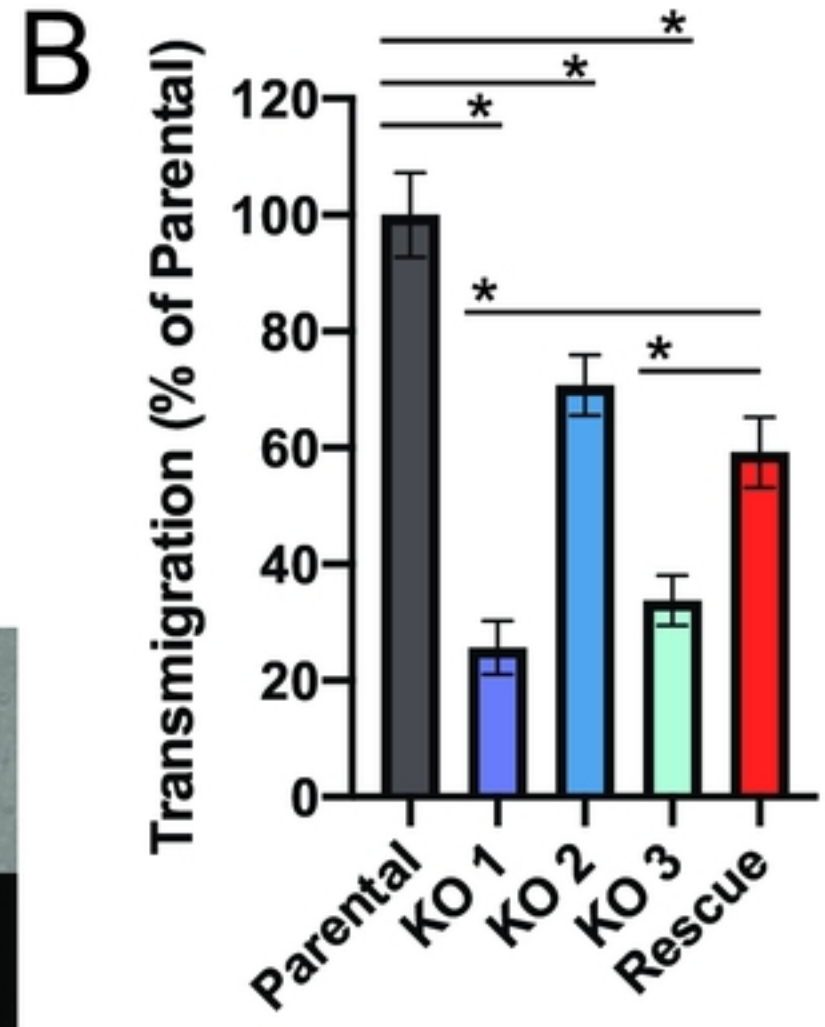
B
Transmigration (% of Parental)
120
100
80
60
40
20
0
*
Parental
KO 1
KO 2
KO 3
Rescue

Fig6